nature neuroscience

ARTICLES

https://doi.org/10.1038/s41593-021-00924-3



# Pain induces adaptations in ventral tegmental area dopamine neurons to drive anhedonia-like behavior

Tamara Markovic[1,2,3,4], Christian E. Pedersen[5,6], Nicolas Massaly[1,2,3], Yvan M. Vachez[1,2,3], Brian Ruyle[1,2,3], Caitlin A. Murphy[1], Kavitha Abiraman[1], Jung Hoon Shin[7], Jeniffer J. Garcia[3], Hye Jean Yoon[1,2,3], Veronica A. Alvarez[7], Michael R. Bruchas[5,6], Meaghan C. Creed[1,2,3,4,8,9,10] ✉ and Jose A. Morón[1,2,3,4,8,10] ✉

**The persistence of negative affect in pain leads to co-morbid symptoms such as anhedonia and depression—major health issues in the United States. The neuronal circuitry and contribution of specific cellular populations underlying these behavioral adaptations remains unknown. A common characteristic of negative affect is a decrease in motivation to initiate and complete goal-directed behavior, known as anhedonia. We report that in rodents, inflammatory pain decreased the activity of ventral tegmental area (VTA) dopamine (DA) neurons, which are critical mediators of motivational states. Pain increased rostromedial tegmental nucleus inhibitory tone onto VTA DA neurons, making them less excitable. Furthermore, the decreased activity of DA neurons was associated with reduced motivation for natural rewards, consistent with anhedonia-like behavior. Selective activation of VTA DA neurons was sufficient to restore baseline motivation and hedonic responses to natural rewards. These findings reveal pain-induced adaptations within VTA DA neurons that underlie anhedonia-like behavior.**

Pain is a complex phenomenon composed of sensory and emotional affective components[1,2]. As pain persists, the presence of negative affective states can lead to the development of negative emotional states such as anhedonia, anxiety and depression[3,4]. While current pharmacological therapies provide high potency in alleviating sensory disturbances, the negative affective states accompanying pain remain undertreated[5]. Emerging evidence from human and preclinical studies show that there are deficits in emotional decision-making, reward evaluation and reward seeking, or motivation in pain states[6–9]. These deficits can lead to the development of anhedonia and depression[8–10]. Uncovering the neuronal circuitry mediating these pain-induced negative affective states may provide opportunities to develop safer therapies for pain treatment and limit the development of co-morbid disorders.

The mesolimbic DA pathway, composed of DA input from the VTA projecting to the nucleus accumbens (NAc), has a prominent role in reward processing and motivated behavior[11–13]. Neuroimaging studies have revealed that DA release and DA receptor activation are reduced in the NAc in patients experiencing pain[14–16]. This is consistent with animal studies demonstrating a decrease in evoked DA release in the NAc in both inflammatory and neuropathic pain[17,18]. Pain-induced negative affect is also associated with adaptations in the dynorphin neurons in the NAc, which are under potent control of DA release at the axon terminals[19]. While these alterations in DA transmission may explain the impaired motivated responses to natural and drug rewards observed in rodents experiencing pain[17,19,20], the exact mechanisms by which VTA DA neurons are mediating pain-induced adaptations in the mesolimbic pathway remain to be elucidated.

One of the main regulators of VTA DA neuron activity are inhibitory GABAergic inputs. These arise from the rostromedial tegmental nucleus (RMTg), the NAc, the ventral pallidum and the bed nucleus of stria terminalis, among others, and they make up the majority of the synaptic input[21]. RMTg GABAergic inputs are highly controlled by the opioid receptor system, which is downregulated in the presence of pain[17,21,22]. Thus, the focus of this study was to assess the effects of pain on VTA DA circuit dynamics and physiology, to investigate whether these changes lead to maladaptive decrease in motivation for natural rewards (a hallmark of anhedonia-like behavior) and the contribution of inhibitory RMTg GABAergic inputs in mediating these effects.

Using in vivo fiber photometry and ex vivo patch-clamp electrophysiology, we report that in rats, the reduced motivation induced by pain is associated with decreased excitability and reduced activity of VTA DA neurons. This decreased excitability of VTA DA neurons is associated with increased inhibitory drive from GABAergic RMTg afferents. Furthermore, we report that chemogenetic activation of NAc-projecting DA neurons in the VTA is sufficient to overcome the pain-induced reduction in motivated behavior. Finally, pain-associated decrease in sucrose consumption was reversed by

[1]Department of Anesthesiology, Washington University in St. Louis, St. Louis, MO, USA. [2]Pain Center, Washington University in St. Louis, St. Louis, MO, USA. [3]School of Medicine, Washington University in St. Louis, St. Louis, MO, USA. [4]Department of Neuroscience, Washington University in St. Louis, St. Louis, MO, USA. [5]Center for the Neurobiology of Addiction, Pain and Emotion, Departments of Anesthesiology and Pharmacology, University of Washington, Seattle, WA, USA. [6]Department of Bioengineering, University of Washington, Seattle, WA, USA. [7]Laboratory on Neurobiology of Compulsive Behaviors, National Institute on Alcohol Abuse and Alcoholism, Center on Compulsive Behaviors, Intramural Research Program, NIH, Bethesda, MD, USA. [8]Department of Psychiatry, Washington University in St. Louis, St. Louis, MO, USA. [9]Department of Biomedical Engineering, Washington University in St. Louis, St. Louis, MO, USA. [10]These authors contributed equally: Meaghan C. Creed, Jose A. Morón. ✉e-mail: meaghan.creed@wustl.edu; jmoron-concepcion@wustl.edu

inhibiting RMTg GABAergic input onto the VTA, overcome by increasing the concentration of the sucrose reward, and mimicked in naive animals by chemogenetic stimulation of RMTg GABA neurons. Together, these results indicate that the experience of pain decreases the activity and excitability of VTA DA neurons, which are partially driven by an increased inhibitory drive from the RMTg; this blunted VTA DA activity then contributes to pain-induced negative affective states. Our findings represent a crucial step in understanding the neural mechanisms underlying the emotional component of pain and may provide novel targets for the treatment of pain-induced negative affect.

## Results

**Pain suppresses VTA DA neuron activity and alters the dynamics of DA cell firing during motivated behavior.** To assess the effect of pain on the activity of VTA DA neurons during motivated behavior, we employed calcium imaging using in vivo fiber photometry during sucrose self-administration. A progressive ratio (PR) schedule of reinforcement for sucrose was used to assess the motivation of rats[23]. During this test, the number of lever presses necessary to obtain the subsequent reward exponentially increases. Thus, the number of rewards obtained during the PR session provides a direct measure of the motivational state of the animal[23,24].

To selectively record DA neuron calcium transients during this task, we injected a Cre-dependent calcium sensor (AAV-DJ-EF1a-DIO-GCaMP6s) and implanted an optic fiber in the VTA of rats expressing Cre recombinase in tyrosine hydroxylase (TH)-positive (TH-Cre) neurons (Fig. 1a,b and Extended Data Fig. 1a–c). Calcium transients from VTA-infected cells were recorded during the last day of each training session on fixed ratio (FR) schedules FR1, FR2 and FR5 (where one, two and five lever presses, respectively, result in a reward delivery) and PR sessions (Fig. 1 and Supplementary Fig. 1). To assess the impact of pain on the calcium transients of VTA DA neurons, animals received an intraplantar injection of either complete Freund's adjuvant (CFA) as a model of inflammatory pain or saline as a control following the baseline PR session (Fig. 1a and Extended Data Fig. 2f,g).

The number of local maxima of DA calcium transients per minute (the frequency of DA transients) throughout an entire PR2 session was significantly decreased 48 h after the CFA injection compared to baseline (Fig. 1c,i and Extended Data Fig. 2j). These results indicate that pain diminishes the overall frequency of calcium transients in VTA DA neurons during a motivational task, which coincides with a decrease in motivation for natural rewards. Interestingly, the event rate in saline-injected animals remained unchanged, which suggests that repeating the PR session does not alter the overall frequency of VTA DA neurons transients (Fig. 1c,i and Extended Data Fig. 2h).

As previously reported[19], CFA injection diminished the motivation for sucrose rewards, which was measured as a decrease in the number of pellets obtained during the PR2 session (Fig. 1h and Extended Data Fig. 2i,k). Importantly, DA activity during reward-seeking behavior (VTA DA activity aligned to a correct lever press) was not significantly changed 48 h after CFA or saline injection compared to the respective baseline session (Extended Data Fig. 2a–e). However, phasic DA activity associated with the reward delivery was significantly increased 48 h after the administration of CFA relative to baseline (pre-CFA) recordings (Fig. 1d–g,j). This finding suggests that pain enhances the phasic VTA DA neuron activity in response to a given reward.

To assess the persistence of pain effect on motivation and DA neuron activity, we tested the same parameters 1 week after CFA injection. Interestingly, while CFA-induced hyperalgesia persisted at 1 week after the injection, the motivation of the animals for sucrose rewards was restored (Supplementary Fig. 2c,d,j). Consistent with this, overall VTA DA neuron calcium activity and phasic responses aligned to reward delivery were also restored to baseline levels (Supplementary Fig. 2a,b,e–i). This finding further supports the conclusion that a reduction in spontaneous calcium activity in VTA DA neurons is tightly associated with the effects of pain on motivated behavior.

**Pain decreases the intrinsic excitability of VTA DA cells and increases the inhibitory drive onto them.** To dissect the physiological mechanisms underlying the overall decrease in the frequency of VTA DA calcium transients during pain as described above, we used ex vivo patch-clamp recordings from rats injected with CFA or saline (Fig. 2a). VTA DA neurons were identified by a cellular capacitance of >30 pF, spontaneous firing below 5 Hz and the presence of a hyperpolarization-activated cation current, $I_h$ (refs. [25,26]) (Fig. 2a). We found that the resting membrane potential (RMP) of DA neurons was lower in slices from CFA-injected rats compared to saline-injected controls, making VTA DA cells hyperpolarized in the CFA group (Fig. 2b and Extended Data Fig. 3b). We assessed the contribution of inhibitory inputs to this decrease in excitability via bath application of the $GABA_A$ receptor antagonist picrotoxin (PTX) onto the slice. While the application of PTX had negligible effects on the control saline group, it depolarized the VTA DA cells from the CFA group to levels comparable to saline-treated animals (Fig. 2b and Extended Data Fig. 3b). In addition, the rheobase, calculated by injecting a ramp of current to determine the minimum amount of current required to generate an action potential, was significantly higher in CFA-injected animals (Fig. 2c and Extended Data Fig. 3c). This effect was also abolished after the application of PTX (Fig. 2c and Extended Data Fig. 3c). Given that there was no effect of either CFA or PTX on the action potential threshold (Extended Data Fig. 3a), this result suggests that VTA DA neurons from CFA-injected rats receive higher GABAergic inhibition, which results in hyperpolarization and a greater current required to reach action potential threshold. We further characterized the intrinsic excitability of VTA DA neurons by examining the input–output curves from animals injected with CFA or saline. Input–

**Fig. 1 | CFA decreases the frequency of VTA DA neuron calcium transients but amplifies the phasic response to reward. a**, Schematic representation of the viral injection and behavioral methodology. **b**, Representative image of optic fiber placement and VTA DA neurons expressing GCaMP (green). **c**, Representative $Ca^{2+}$ transients of VTA DA neurons during the entire baseline (gray) and post-saline (SAL; left) and post-CFA (right) PR sessions of sucrose self-administration. **d**, Representative heatmaps of fluorescence aligned to the reward delivery (time point 0) for baseline (left) and post-SAL (right) PR sessions for the same animal. **e**, Mean fluorescence aligned to reward delivery for baseline and post-SAL PR sessions ($n=5$ rats; data presented as the mean ± s.e.m.). **f**, Representative heatmaps of fluorescence aligned to the reward delivery (time point 0) for baseline (left) and post-CFA (right) PR sessions for the same animal. **g**, Mean fluorescence aligned to reward delivery for baseline and post-CFA PR sessions ($n=7$ rats; data presented as the mean ± s.e.m.). **h**, Pain decreases the motivation for sucrose rewards (two-way ANOVA for repeated measures, time: $F_{1,10}=16.08$, $P=0.0025$; interaction (time × treatment): $F_{1,10}=4.143$, $P=0.0692$; Sidak's post hoc between PR2 and PR1: $CFA_{(n=7)}$, $^{**}P=0.0017$; $n=7$ (CFA) or 5 (SAL) rats). **i**, Pain diminishes the frequency of calcium transients of VTA DA neurons (two-tailed Wilcoxon test, $^{*}P=0.0156$; $n=7$ (CFA) or 5 (SAL) rats). **j**, Maximum fluorescence following reward delivery (2–5 s after) is increased in the condition of pain (two-way ANOVA for repeated measures, time: $F_{1,10}=8.520$, $P=0.0047$; interaction (time × treatment): $F_{1,10}=2.490$, $P=0.1191$; Sidak's post hoc between PR2 and PR1: $CFA_{(n=7)}$, $^{**}P=0.0017$). The data are presented as the mean ± s.e.m.

output curves were generated with 200-ms current steps injected in increments of 10 pA from 0 to 200 pA. Input resistance was not affected by CFA, and while PTX application slightly increased input resistance in CFA-treated animals (Fig. 2d and Extended Data Fig. 3d), the input–output curve was not affected by CFA or the application of PTX, as no groups demonstrated significant differences at

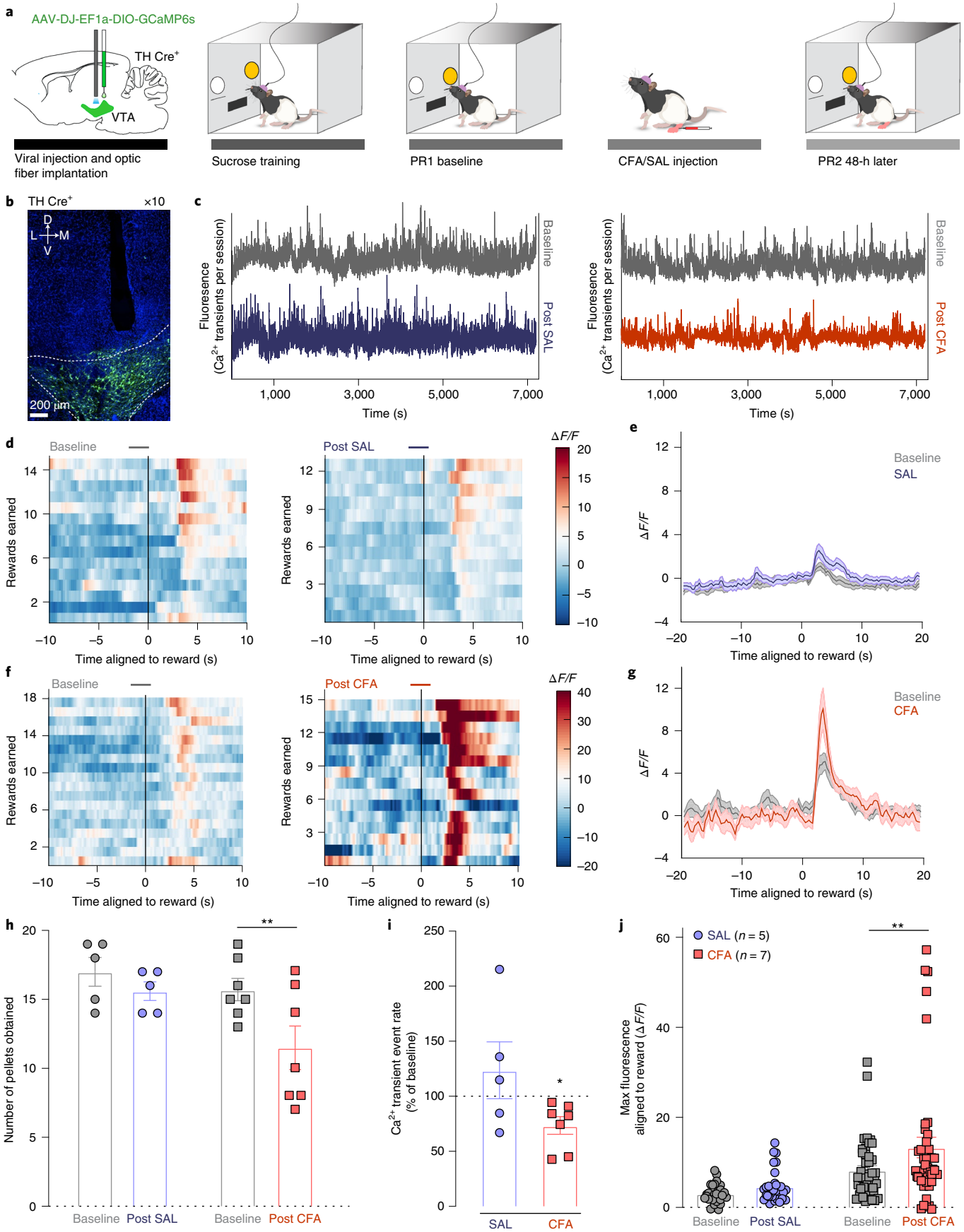

any current steps (Fig. 2g,h). Moreover, the spontaneous firing rate of VTA DA neurons was not significantly lower in CFA-injected mice relative to saline-injected mice, and this was not affected by the application of PTX (Fig. 2e,f). Taken together, our results demonstrate that while the lower intrinsic excitability of VTA DA neurons in pain is mediated through increased GABAergic drive, the lack of effect of PTX on the spontaneous activity of DA cells in pain suggests that additional, GABA-independent, presumably cell-autonomous adaptations, contribute to this decrease in spontaneous activity ex vivo.

To directly test the hypothesis that inhibitory drive is increased onto VTA DA neurons following pain induction, we next measured spontaneous inhibitory postsynaptic currents (IPSCs), which reflect spontaneous neurotransmitter release. We found that the distribution of inter-event intervals (IEIs) of spontaneous IPSCs, but not the amplitude, was significantly decreased in slices from CFA-treated rats (Fig. 2i–k). This CFA-induced increase in the frequency of spontaneous inhibitory events suggests that enhanced pre-synaptic release is occurring, which further supports the conclusion that inhibitory drive onto VTA DA neurons is increased in pain (Fig. 2j).

The electrophysiological changes found at the soma regions of VTA DA neurons indicate decreased activity after the induction of inflammatory pain. These VTA DA neurons send long axonal projections that innervate the NAc shell (NAcSh) regions and release DA. DA transmission in the NAcSh is determined by local synaptic properties in addition to somatic activity of DA neurons[27]. Thus, we next examined whether pain induces changes to the properties of DA release in the NAcSh using fast-scanning cyclic voltammetry (FSCV) to record ex vivo-evoked DA transients from mouse brain slices 48 h after CFA or saline injection. DA transients were evoked using both electrical and optogenetic approaches.

We found a small decrease in the amplitude of the evoked transients in the CFA-injected mice at submaximal stimulations (Supplementary Fig. 3c), which is indicative of a small impairment in the ability to electrically evoke DA release at the synaptic terminal following the induction of pain. However, other properties of DA release remained largely unaffected by pain (Supplementary Fig. 3a,b,d–j).

Taken together, these findings reveal that increased GABAergic inhibition following CFA treatment contributes to the decreased excitability of VTA DA neurons. Meanwhile, the properties of the DA release in the NAcSh projection site are unaffected by CFA injection.

**Chemogenetic activation of VTA–NAc-projecting DA neurons is sufficient to reverse pain-induced decrease in motivation.** Our photometry data indicate that pain-induced impairment in VTA DA cell activity occurs in parallel with a decrease in motivation for sucrose rewards. Thus, we hypothesized that in vivo activation of VTA DA neurons would be sufficient to reverse pain-induced deficits in motivated behavior. To investigate this, we utilized chemogenetics in combination with PR sucrose self-administration. To selectively activate VTA DA neurons, we bilaterally injected Cre-dependent excitatory designer receptors exclusively activated by designer drugs (DREADDs) (AAV5-hSyn-DIO-hM3D(Gq)-mCherry) or control virus (AAV5-Ef1a-DIO-mCherry) in the VTA of TH-Cre rats (Fig. 3a,b and Extended Data Figs. 4c and 5a).

First, we assessed whether clozapine-*N*-oxide (CNO) application led to an increase in DREADD-expressing DA neuron activation using cFos expression as a proxy for neuronal activation. We demonstrated that both control and DREADD viral expression were highly restricted to TH-positive (DA) neurons in the VTA (Supplementary Fig. 4a,b). Moreover, we observed that around 70% of TH-positive neurons expressing DREADDs were co-labeled with cFos, while control groups showed a significantly lower co-labeling and overall expression of cFos (Supplementary Fig. 4c). This result further substantiates the high selectivity of DREADD-expressing neuronal activation after CNO administration.

Utilizing this approach, we found that activation of DREADD-expressing DA neurons, via subcutaneous (s.c.) injection of CNO (1 mg per kg) during the PR2 session, was sufficient to reverse the CFA-induced decrease in motivation for the self-administration of sucrose pellets. That is, there was no difference between CFA-treated or saline-injected animals after chemogenetic activation of VTA DA cells (Fig. 3c). Importantly, CFA control groups injected with DREADD virus or CNO alone demonstrated a decrease in motivation for sucrose pellets on the second PR test (as measured by the decreased number of pellets obtained). This confirms the observation that restoration of motivation is tightly associated with VTA DA neuron activation (Fig. 3c and Extended Data Fig. 4a). Additionally, chemogenetic activation of VTA DA neurons increased the motivation for sucrose pellets in saline-injected animals, as shown by the increase in number of the rewards obtained during the PR2 task compared to the baseline sessions, which has been previously reported[28]. Moreover, the restoration of motivation in CFA-injected animals did not appear to be mediated through an overall increase in locomotor activity, as locomotion was only

**Fig. 2 | VTA DA cells are hyperpolarized in CFA-injected animals, exhibiting decreased intrinsic excitability and increased inhibitory drive onto them.** **a**, Top: schematic and representative picture of a patch pipette onto the soma of a VTA DA neuron. Bottom: identification of DA neurons was made by the presence of a large hyperpolarization-activated inward current, $I_h$. **b**, The RMP is lower in the CFA-treated group. Application of PTX restores RMP to the level of saline-injected animals (two-way ANOVA for repeated measures, treatment (PTX): $F_{1,42}=13.36$, $P=0.0007$; interaction (treatment (PTX) × treatment (CFA/SAL)): $F_{1,42}=10.50$, $P=0.0023$; Sidak's post hoc between CFA and SAL: $^{**}P=0.0046$ at baseline, Sidak's post hoc between PTX and baseline: CFA, $^{****}P<0.0001$, $n=21$ cells from 5 rats (SAL) or 23 cells from 4 rats (CFA)). **c**, The amount of current necessary to evoke the first action potential is higher in CFA-treated rats. This effect is eliminated after application of PTX (two-way ANOVA for repeated measures, treatment (PTX): $F_{1,40}=1.327$, $P=0.2562$; interaction (treatment (PTX) × treatment (CFA/SAL)): $F_{1,40}=6.113$, $P=0.0178$; Sidak's post hoc between CFA and SAL: $^{**}P=0.0021$ at baseline, Sidak's post hoc between PTX and baseline: CFA, $^{*}P=0.0242$, $n=20$ cells from 5 rats (SAL) or 23 cells from 4 rats (CFA)). **d**, CFA does not alter input resistance (RIN), while the application of PTX increases input resistance in the CFA-treated animals (two-way ANOVA for repeated measures, treatment (PTX): $F_{1,42}=3.037$, $P=0.0887$; interaction (treatment (PTX) × treatment (CFA/SAL)): $F_{1,42}=3.520$, $P=0.0676$; Sidak's post hoc between PTX and baseline: CFA, $^{*}P=0.0243$, $n=21$ cells from 5 rats (SAL) or 23 cells from 4 rats (CFA)). **e**, Representative traces of spontaneous activity. **f**, Spontaneous firing rates of VTA DA neurons show no statistically significant difference in pain ($n=21$ cells from 5 rats (SAL) or 23 cells from 4 rats (CFA)). **g**, Representative input–output traces. **h**, The input–output curve of neuronal excitability is not altered by pain or PTX ($n=12$ cells from 5 rats (SAL) or 14 cells from 4 rats (CFA)). **i**, Representative traces of spontaneous IPSCs. **j**, The frequency of spontaneous IPSCs is increased in the condition of pain, which is indicative of an increased inhibitory drive onto VTA DA neurons. Inset shows the distribution of cumulative probability for the IEI represented as the mean ± s.e.m. (Kolmorogov–Smirnov test = 4.925, $^{***}P=0.001$; mean IEI: $^{****}P<0.0001$, two-tailed Mann–Whitney test, $n=27$ from 5 rats (SAL) or 25 from 5 rats (CFA)). **k**, The mean amplitude of spontaneous IPSCs is not altered by pain. Inset show the distribution of cumulative probability for Amp represented as the mean ± s.e.m. (Kolmorogov–Smirnov test = 1.196, $P=0.114$ (NS, not significant); mean Amp: $P=0.159$ (NS), two-tailed Mann–Whitney test, ($n=27$ from 5 rats (SAL) or 25 from 5 rats (CFA)). The data are presented as the mean ± s.e.m.

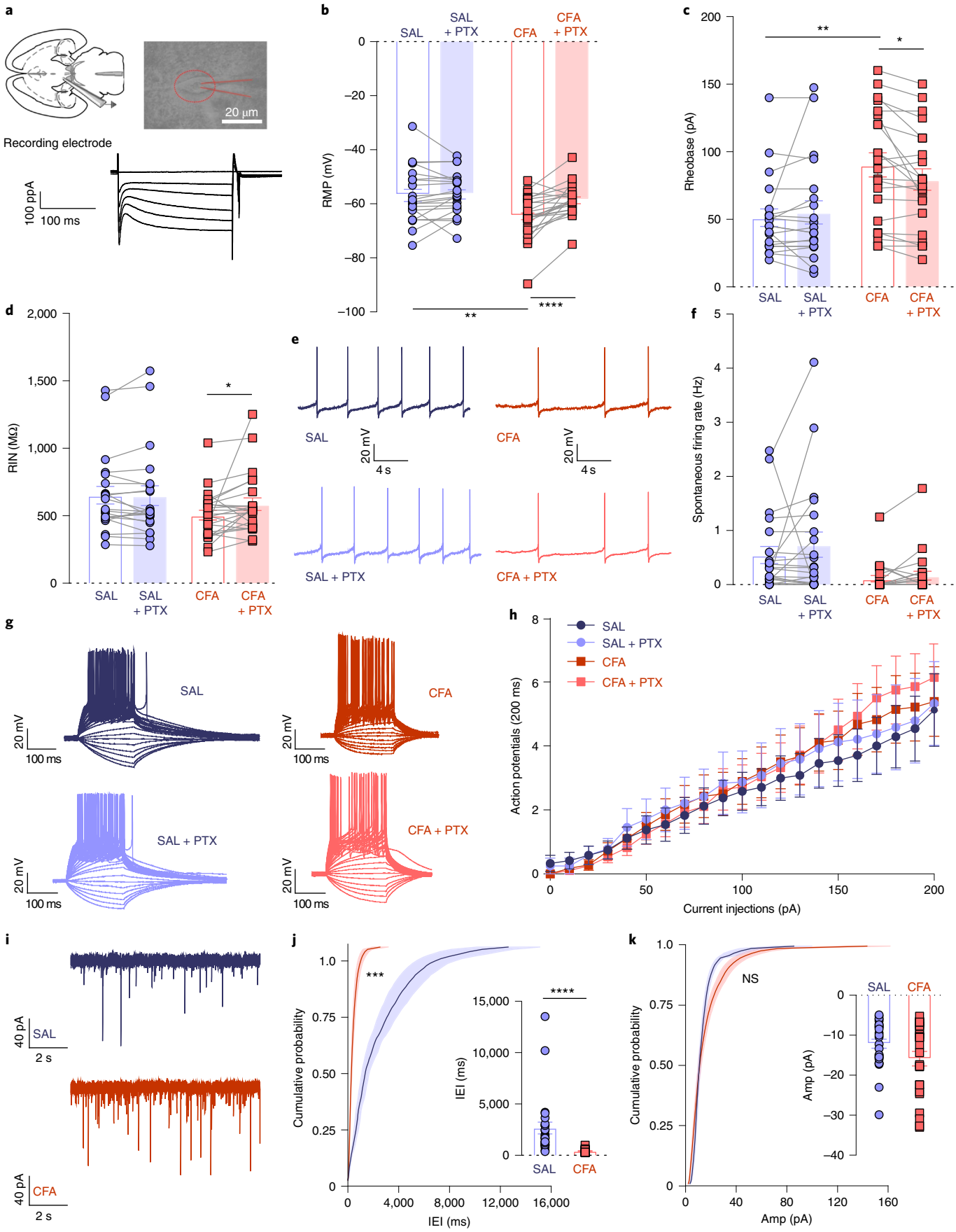
a
Recording electrode
20 µm
100 ppA
100 ms
b
SAL
SAL + PTX
CFA
CFA + PTX
RMP (mV)
0
−20
−40
−60
−80
−100
**
****
c
Rheobase (pA)
200
150
100
50
0
**
*
SAL
SAL + PTX
CFA
CFA + PTX
d
RIN (MΩ)
2,000
1,500
1,000
500
0
*
SAL
SAL + PTX
CFA
CFA + PTX
e
SAL
CFA
20 mV
4 s
SAL + PTX
CFA + PTX
f
Spontaneous firing rate (Hz)
5
4
3
2
1
0
SAL
SAL + PTX
CFA
CFA + PTX
g
SAL
CFA
SAL + PTX
CFA + PTX
20 mV
100 ms
h
SAL
SAL + PTX
CFA
CFA + PTX
Action potentials (200 ms)
8
6
4
2
0
0
50
100
150
200
Current injections (pA)
i
40 pA
SAL
2 s
CFA
j
Cumulative probability
1.0
0.75
0.50
0.25
0
***
IEI (ms)
15,000
10,000
5,000
0
****
SAL
CFA
0
4,000
8,000
12,000
16,000
IEI (ms)
k
Cumulative probability
1.0
0.75
0.50
0.25
0
NS
Amp (pA)
0
−10
−20
−30
−40
SAL
CFA
0
40
80
120
160
Amp (pA)

increased in saline-treated animals after DREADD activation, but not in CFA-treated animals (Supplementary Fig. 5a–c).

The VTA–NAc mesolimbic pathway is a key circuit encoding motivational processes[11,12,29], with the NAcSh mediating both aversive stimuli such as pain and motivational salience[19,27,30]. Thus, we next investigated whether activation of VTA neurons projecting to the NAcSh would be sufficient to reverse the pain-induced decrease in motivation for sucrose. Wild-type rats were injected with a retrograde canine adenovirus carrying Cre recombinase (CAV2-Cre)[31] in the NAcSh and a Cre-dependent excitatory DREADD (AAV5-hSyn-DIO-hM3D(Gq)-mCherry), or a control virus (AAV5-Ef1a-DIO-mCherry), in the VTA (Fig. 3e,f and Extended Data Figs. 4d and 5b). Chemogenetic activation of VTA to NAcSh projection neurons was sufficient to reverse the CFA-induced decrease in rewards obtained during the PR2 task, whereas it had no effect in control (saline-treated) animals (Fig. 3g and Extended Data Fig. 4b). Furthermore, we observed a significant bimodal distribution of the performance of the animal during the PR2 session in the CFA group, with a cluster of animals whose motivation was decreased and a cluster of animals with minimal change in motivation (Fig. 3i–k and Extended Data Fig. 4e). Importantly, the percent of motivation change was correlated with the infection rate of the virus (Fig. 3i–k).

Since previous work has demonstrated that pain relief induced by local anesthetic enhances DA transmission in the VTA–NAcSh pathway[32], we next assessed whether our chemogenetic approaches produced analgesia and could have restored motivation for sucrose seeking. Thus, we measured thermal hyperalgesia using the Hargreaves test. Neither general enhancement of the VTA DA neurons nor selective activation of the VTA–NAcSh pathway reversed CFA-induced hyperalgesia (Fig. 3d,h). Together, these results indicate that selective activation of the mesolimbic VTA–NAc pathway or VTA DA neurons is sufficient to reverse the observed pain-induced decrease in motivated behavior without affecting the sensory component of inflammatory pain.

Last, to assess whether increasing the activity of DA neurons within the VTA–NAcSh pathway specifically restores motivation in the condition of pain, we bilaterally injected a Cre-dependent excitatory DREADD (AAV5-hSyn-DIO-hM3D(Gq)-mCherry) or control virus (AAV5-Ef1a-DIO-mCherry) in the VTA of TH-Cre rats and implanted an intra-NAcSh cannula for the microinjection of 1 mM of CNO or artificial cerebrospinal fluid (aCSF) (Fig. 4a,b and Extended Data Fig. 6b,c). Chemogenetic enhancement of NAcSh-projecting VTA DA terminals reversed the CFA-induced decrease in motivation for sucrose rewards without altering CFA-induced hyperalgesia (Fig. 4c,d and Extended Data Fig. 6a), whereas it had no effect in control (saline) rats. This finding further strengthens the hypothesis that restoring DA neurotransmission selectively within the NAcSh is necessary to restore motivation for sucrose following CFA treatment.

**Increasing the hedonic value of natural reward overcomes the effects of pain on sucrose consumption.** We previously demonstrated that pain induces a rightward shift in the opioid dose response, which suggests that there is an impairment in the rewarding properties of opioid drugs[17]. Therefore, we next examined whether pain also alters the rewarding properties for natural (in this case, sucrose) rewards. We employed a two-bottle choice paradigm[33] in which an animal can freely choose between water or a sucrose solution for 1 h. This paradigm enabled us to investigate the effect of pain on reward consumption, whereby we could alter the hedonic value of the reward by using escalating concentrations of sucrose in separate testing sessions. To ensure that the sucrose concentrations used in the two-bottle choice were not perceived as aversive, we measured orofacial reactivity such as consummatory protrusions and hedonic licks for 5%, 30% and 60% sucrose in naive animals (Extended Data Fig. 7a and Supplementary Videos 1 and 2). We found that 5% and 30% sucrose significantly increased consummatory protrusions compared to water, whereas this was not significant for the 60% sucrose solution (Extended Data Fig. 7a). In addition, 60% sucrose elicited exaggerated swallowing, possibly due to the increased viscosity of the solution. This behavior is easily distinguishable from aversive gapes induced by quinine (Supplementary Videos 1, 2 and 3). These data demonstrate that the concentrations used in the two-bottle choice experiments are not aversive and produce similar orofacial responses.

CFA-injected and saline-injected animals underwent 4 days of habituation during which they were simultaneously exposed to a 5% sucrose solution and a water bottle (Fig. 5a). Then, a baseline test was performed in which sucrose (5%, 30% or 60%) and water volume consumed were recorded. Subsequently, CFA or saline was injected into the hindpaw of the rat and a second two-bottle choice

**Fig. 3 | Chemogenetic activation of VTA DA neurons, or the VTA–NAc pathway, reverses the CFA-induced decrease in motivation. a**, Schematic representation of the viral injection and behavioral methodology. HPC, hippocampus; PFC, prefrontal cortex; VEH, vehicle. **b**, Representative coronal section of VTA Gq DREADD-expressing neurons. Blue, 4,6-diamidino-2-phenylindole (DAPI); red, mCherry (Gq DREADD); green, TH (DA neurons). **c**, Activation of DA-containing neurons in the VTA reverses the CFA-induced decrease in motivation for sucrose pellets. Animals injected with control virus and CNO alone showed decreases in motivation after the CFA injection (two-way ANOVA for repeated measures, time: $F_{1,47} = 46.35$, $P < 0.0001$; interaction (time × treatment): $F_{3,47} = 45.18$, $P < 0.0001$; Sidak's post hoc between groups during PR2: hM3Dq + CFA + $VEH_{(n=10)}$ versus hM3Dq + SAL + $CNO_{(n=14)}$, $^{\$\$\$\$}P < 0.0001$, hM3Dq + CFA + VEH versus hM3Dq + CFA + $CNO_{(n=17)}$, $^{\#\#\#\#}P < 0.0001$; mCherry + CFA + $CNO_{(n=10)}$ versus hM3Dq + SAL + CNO, $^{\$\$\$\$}P < 0.0001$, mCherry + CFA + CNO versus hM3Dq + CFA + CNO, $^{\#\#\#\#}P < 0.0001$). **d**, CFA-induced hyperalgesia (schematic on top left) is not altered by the activation of DA-containing neurons in the VTA (two-way ANOVA for repeated measures, time: $F_{2,94} = 507.2$, $P < 0.0001$; interaction (time × treatment): $F_{6,94} = 59.72$, $P < 0.0001$; Sidak's post hoc for each group compared to the group's baseline session: $^{****}P < 0.0001$). **e**, Schematic representation of the viral injection and behavioral methodology. WT, wild type. **f**, Representative coronal section of VTA Gq DREADD-expressing neurons. Blue, DAPI; red, mCherry (Gq DREADD); green, TH (DA neurons). **g**, The activation of NAcSh-projecting VTA neurons restores motivation in CFA-treated aniamls. Control CFA animals injected with either CNO or virus alone show decreases in motivation (two-way ANOVA for repeated measures, time: $F_{1,53} = 148.4$, $P < 0.0001$; interaction (time × treatment): $F_{3,53} = 14.66$, $P < 0.0001$; Sidak's post hoc during PR2 between the groups: hM3Dq + CFA + $VEH_{(n=17)}$ versus hM3Dq + SAL + $CNO_{(n=12)}$, $^{\$\$\$}P = 0.0004$, hM3Dq + CFA + VEH versus hM3Dq + CFA + $CNO_{(n=17)}$, $^{\#\#}P = 0.0085$; mCherry + CFA + $CNO_{(n=11)}$ versus hM3Dq + SAL + CNO, $^{\$\$}P = 0.0024$, mCherry + CFA + CNO versus hM3Dq + CFA + CNO, $^{\#}P = 0.0344$). **h**, CFA-induced hyperalgesia is not altered by activation of VTA-NAc pathway (two-way ANOVA for repeated measures, time: $F_{2,106} = 597.4$, $P < 0.0001$; interaction (time × treatment): $F_{6,106} = 74.90$, $P < 0.0001$; Sidak's post hoc for each group as compared to the group's baseline session: $^{****}P < 0.0001$). **i**–**k**, Bimodal distribution of the performance of the animal during the second PR session is observed in the hM3Dq + CFA + CNO test group ($P = 0.0312$, Hartigan dip test, number of shuffles 20,000). The percent of motivation change is corelated with the infection rate of the virus. **i**, The total number of VTA-NAc mCherry-expressing neurons: $r = 0.6292$, $P = 0.0068$, $n = 17$ rats, Spearman correlation test. **j**, The number VTA-NAc mCherry-expressing TH-positive neurons: $r = 0.7446$, $P = 0.0006$, $n = 17$ rats, Spearman correlation test. **k**, The number of mCherry-expressing TH-negative neurons: $r = 0.539$, $P = 0.0256$, $n = 17$ rats, Spearman correlation test. The data are presented as the mean ± s.e.m.

test was performed 48 h later (Fig. 5a). We found that animals in the CFA group decreased their voluntary consumption of 5% and 30% sucrose solution relative to the baseline test, whereas control saline-injected animals did not (Fig. 5b,c,e). The amount of water consumed was unchanged between the experimental groups, which indicates that the observed changes in drinking behavior are specific to sucrose consumption and reflect an impairment in the perceived hedonic value of sucrose reward in pain (Extended Data Fig. 7b,c,d). Furthermore, there was no significant difference in sucrose consumption between CFA-treated animals and saline-injected animals when the concentration was increased to 60% (Fig. 5d,e). These data indicate that pain alters the rewarding properties only for lower reward values but does not affect reward consumption when the sucrose value is increased, thereby indicating a rightward shift in the hedonic value of sucrose.

Last, using a chemogenetic approach, we found that selective activation of VTA DA neurons is sufficient to reverse the CFA-induced decrease in motivated behavior (Fig. 3). Thus, we

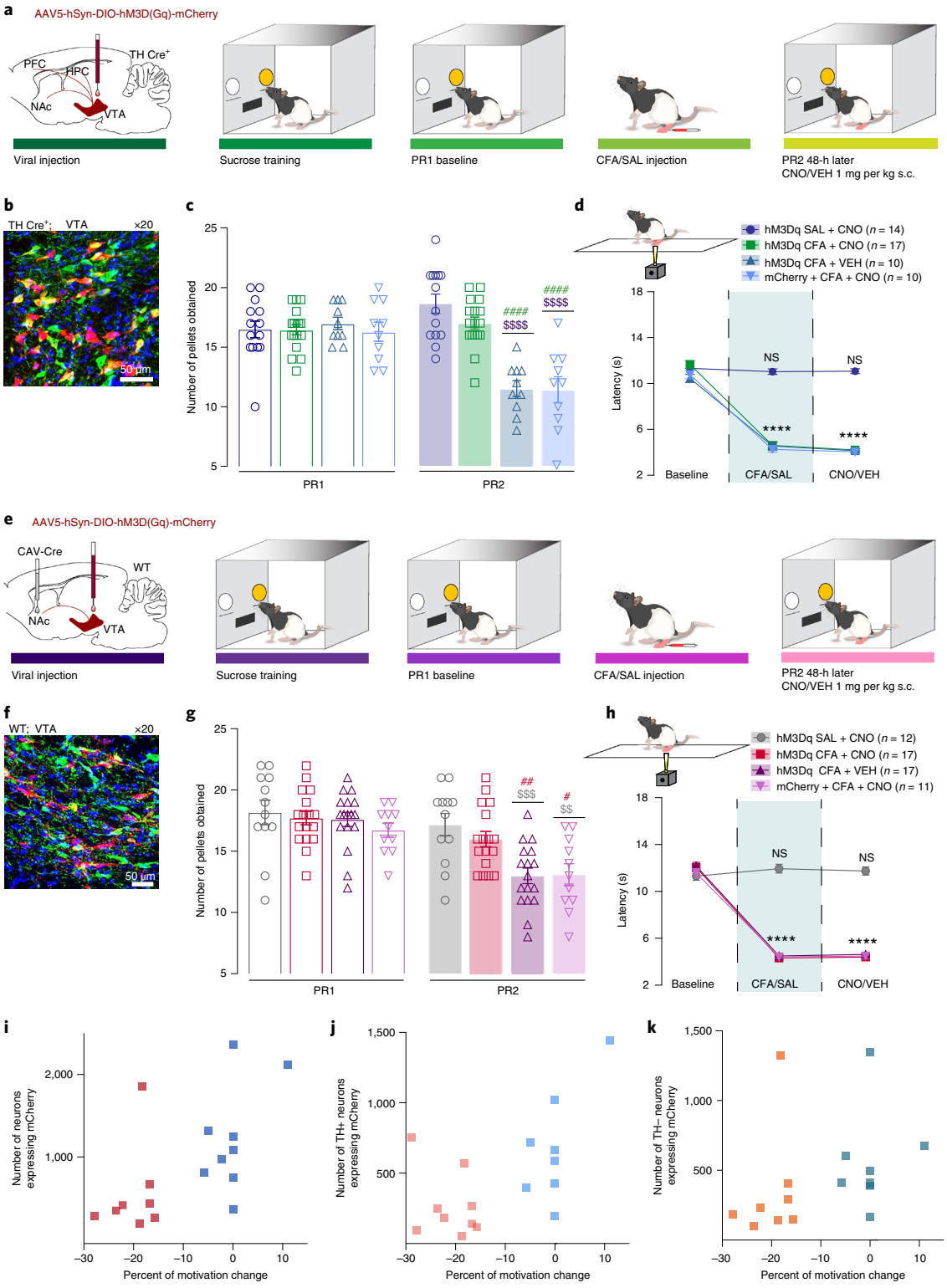

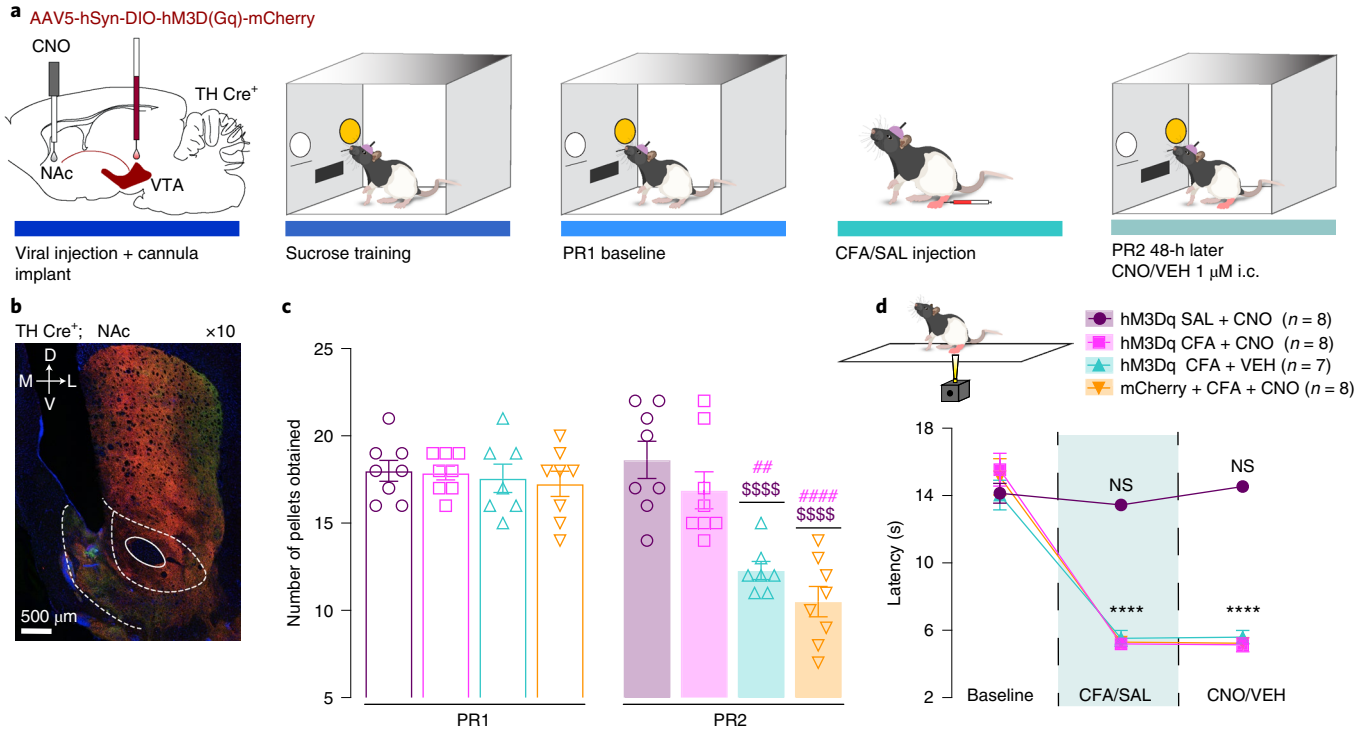


**Fig. 4 | Chemogenetic activation of NAcSh-projecting VTA DA neurons mitigates the effect of CFA on motivated behavior. a**, Schematic representation of the viral injection and behavioral methodology. **b**, Representative coronal section of NAcSh cannula placement and terminal expression of DREADDs injected in the VTA of TH-Cre rats. Blue, DAPI; red, mCherry (Gq DREADD); green, TH (DA neuron terminals). The lines delineate nucleus accumbens core and shell region. The solid line depicts anterior commissure (ac). The complete oval dashed line depicts nucleus accumbens core (NAcCr; the area between the ac and NAcSh), and the medial curved dashed line depicts nucleus accumbens shell (NAcSh; the area surrounding NAcCr). **c**, Chemogenetic enhancement of VTA–NAcSh-projecting DA neurons reverses the CFA-induced decrease in motivation (two-way ANOVA for repeated measures, time: $F_{1,27} = 53.97$, $P < 0.0001$; interaction (time × treatment): $F_{3,27} = 17.31$, $P < 0.0001$; Sidak's post hoc during PR2 between the groups: hM3Dq + CFA + $VEH_{(n=7)}$ versus hM3Dq + SAL + $CNO_{(n=8)}$, $^{\$\$\$\$}P < 0.0001$, hM3Dq + CFA + VEH versus hM3Dq + CFA + $CNO_{(n=8)}$, $^{\#\#}P = 0.0012$; mCherry + CFA + $CNO_{(n=8)}$ versus hM3Dq + SAL + CNO, $^{\$\$\$\$}P < 0.0001$, mCherry + CFA + CNO versus hM3Dq + CFA + CNO, $^{\#\#\#\#}P < 0.0001$). **d**, Chemogenetic enhancement of VTA–NAcSh-projecting DA neurons does not alter CFA-induced hyperalgesia (schematic on top left) (two-way ANOVA for repeated measures, time: $F_{2,54} = 233.9$, $P < 0.0001$; interaction (time × treatment): $F_{6,54} = 26.38$, $P < 0.0001$; Sidak's post hoc for each group compared to the group's baseline session: $^{****}P < 0.0001$). The data are presented as the mean ± s.e.m.

assessed whether selective activation of VTA DA neurons could also reverse the CFA-induced decrease in 5% sucrose solution consumption. We bilaterally injected a Cre-dependent excitatory DREADD (AAV5-hSyn-DIO-hM3D(Gq)-mCherry) or control virus (AAV5-Ef1a-DIO-mCherry) in the VTA of TH-Cre rats (Fig. 5f and Extended Data Fig. 8d,e). Selective activation of VTA DA neurons reversed the decrease in 5% sucrose solution consumption in CFA-treated animals, while it had no effect in control (saline-treated) animals (Fig. 5g and Extended Data Fig. 8a–c). Importantly, in these conditions, a decrease in the amount of sucrose consumed was still observed in our CFA control groups injected with either DREADD virus or CNO alone (Fig. 5g). These results indicate that the activation of the VTA DA system is sufficient to restore normal hedonic responses to natural rewards.

**RMTg GABAergic neuronal projections onto VTA DA neurons exhibit higher release probability in pain.** We showed above that in VTA slices from CFA-injected rats, DA cells were less excitable in part due to increased GABAergic inhibition. Inhibition of VTA DA neurons can disrupt reward consumption[34]. Furthermore, the activity of VTA DA neurons is highly controlled by the intrinsic excitability of DA cells and their synaptic inputs[11,21]. The RMTg is one of the main sources of inhibitory drive onto VTA DA neurons[21,35] and is the major opioid-sensitive GABA input onto VTA DA neurons[21]. We previously demonstrated that μ-opioid receptor (MOR)-mediated inhibition of GABA release in the VTA is diminished in pain[17]. Thus, we hypothesized that the RMTg GABA input onto VTA DA neurons is enhanced in the presence of pain.

To test this, we measured the release properties of RMTg GABA neurons using paired-pulse ratio (PPR). GAD-Cre rats were injected with Cre-dependent channel rhodopsin (AAV5-EF1a-DIO-ChR2-eYFP) virus in the RMTg. After 2 weeks of recovery to allow for appropriate viral expression, animals received either CFA or saline injection in the hindpaw (Fig. 6a). RMTg-evoked IPSCs onto VTA DA neurons were recorded ex vivo by activation of ChR2-expressing RMTg terminals (Fig. 6b). Light power was adjusted to the lowest intensity at which we could consistently evoke a post-synaptic response. We found that the PPR was significantly depressed in CFA-treated animals compared to saline-injected controls (Fig. 6c), which demonstrates the increased release probability of RMTg GABA terminals onto VTA DA neurons. Furthermore, the PPR was not correlated with the evoked amplitude of initial response at any inter-pulse interval, which indicates that the observed effect is not an artifact arising from potential vesicle depletion scaling with the efficiency of the channelrhodopsin (Extended Data Fig. 9h–j).

Next, we assessed whether RMTg-mediated inhibition of VTA would mimic the effects of pain on voluntary sucrose consumption.

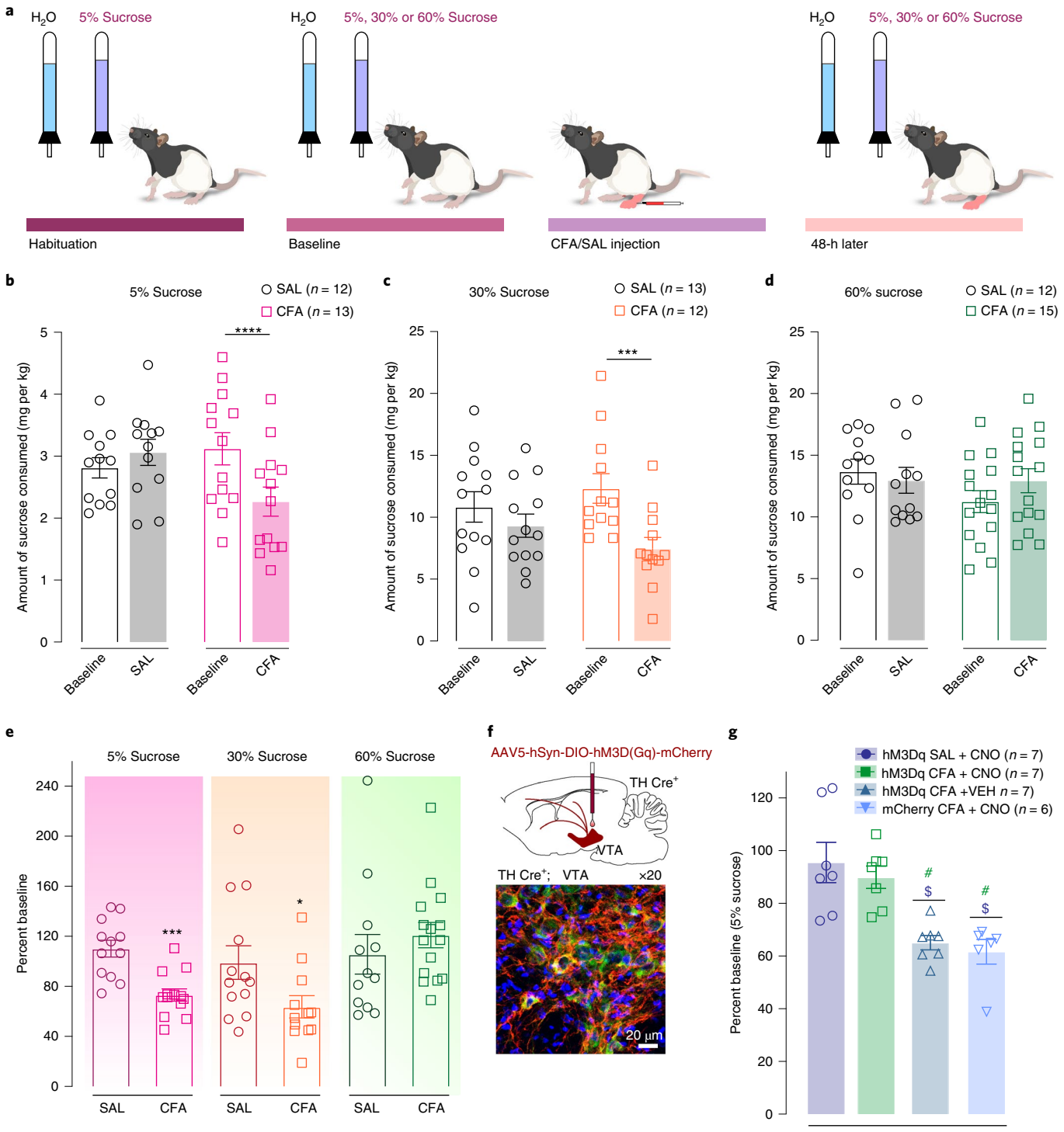


**Fig. 5 | Increasing the concentration of sucrose reward overcomes the effects of CFA on sucrose consumption. a**, Schematic representation of the behavioral methodology. **b**–**d**, CFA induces a significant decrease in the amount of 5% and 30% sucrose consumed (open bars, baseline; filled bars,~48 h post CFA/SAL). **b**, 5% Sucrose two-way ANOVA for repeated measures, time: $F_{1,23} = 6.387$, $P = 0.0188$; interaction (time × treatment): $F_{1,23} = 21.31$, $P = 0.0001$; Sidak's post hoc within group: $CFA_{(n=13)}$ baseline versus 48 h post CFA, $^{****}P < 0.0001$. **c**, 30% Sucrose two-way ANOVA for repeated measures, time: $F_{1,23} = 14.86$, $P = 0.0008$; interaction (time × treatment): $F_{1,23} = 4.105$, $P = 0.0545$; Sidak's post hoc within group: $CFA_{(n=12)}$ baseline versus 48 h post CFA, $^{***}P = 0.0009$). **d**, Increasing the concentration of sucrose solution to 60% prevents the pain-induced decrease in sucrose consumption. **e**, Sucrose consumption presented as the percent change of baseline (5% sucrose, two-tailed unpaired *t*-test between CFA ($n = 13$ rats) and SAL ($n = 12$ rats), $^{***}P = 0.0002$; 30% sucrose, two-tailed unpaired *t*-test between CFA ($n = 12$ rats) and SAL ($n = 13$ rats), $^{*}P = 0.0409$; 60% sucrose (CFA ($n = 15$ rats), SAL ($n = 12$ rats)). **f**, Top: schematic of the viral injection method. Bottom: representative coronal section of VTA Gq DREADD-expressing neurons. Blue, DAPI; red, mCherry (Gq DREADD); green, TH (DA neurons). **g**, Chemogenetic activation of DA-containing neurons in the VTA restores consumption of 5% sucrose in pain (Kruskal–Wallis test, $^{***}P = 0.0005$; two-tailed Dunn's multiple comparisons between groups: hM3Dq CFA + $VEH_{(n=7)}$ versus hM3Dq SAL + $CNO_{(n=7)}$, $^{\$}P = 0.0183$, hM3Dq CFA + VEH versus hM3Dq CFA + $CNO_{(n=7)}$, $^{\#}P = 0.0204$; mCherry CFA + $CNO_{(n=6)}$ versus hM3Dq SAL + CNO, $^{\$}P = 0.0139$, mCherry CFA + CNO versus hM3Dq CFA + CNO, $^{\#}P = 0.0155$). The data are presented as the mean ± s.e.m.

We activated RMTg GABA neurons using a chemogenetic approach during a two-bottle choice experiment. A Cre-dependent excitatory DREADD (AAV5-hSyn-DIO-hM3D(Gq)-mCherry) or control virus (AAV5-Ef1a-DIO-mCherry) was bilaterally injected in the RMTg of GAD-Cre rats (Fig. 6d,e and Extended Data Fig. 9f,g).

After habituation sessions of the two-bottle choice, a baseline test was performed during which both 60% sucrose and water volume consumed were recorded. To maintain consistency with the pain plus two-bottle choice experiments, animals were tested again 48 h later when they received a s.c. administration of CNO (1 mg per kg). A week later, animals underwent another set of baseline and post-CNO sessions using a 5% sucrose concentration in the two-bottle choice test (Fig. 6d).

In this experiment, activation of RMTg GABA neurons was sufficient to induce a decrease in consumption of both 60% and 5% sucrose solutions (Fig. 6f,g and Extended Data Fig. 9e) without altering the volume of water consumed or the preference for sucrose solution over water (Extended Data Fig. 9a–d). This finding shows that enhancing the inhibitory drive onto VTA DA neurons induces a decrease in consumption of 5% sucrose solution, similar to pain-induced anhedonia-like states. The decreased consumption of 60% sucrose in this experiment further demonstrates a role of RMTg GABA neurons in reward processing.

**RMTg GABA cell activity is necessary for pain-induced anhedonia.** Finally, to assess the necessity of enhanced RMTg GABAergic inputs onto the VTA in driving anhedonia-like behaviors, we inhibited this pathway in CFA-injected and in saline-injected animals using chemogenetics during the 5% sucrose two-bottle choice paradigm (Fig. 6h). Here, we bilaterally injected a Cre-dependent inhibitory DREADD (AAV5-hSyn-DIO-hM3D (Gi)-mCherry) or control virus (AAV5-Ef1a-DIO-mCherry) in the RMTg of GAD-Cre rats and implanted an intra-VTA cannula for the local delivery of 1 mM of CNO or aCSF (Fig. 6i and Extended Data Fig. 10d–g). Inhibition of RMTg GABAergic input onto the VTA via intracranial CNO injection restored the consumption of 5% sucrose in the two-bottle choice experiment in CFA-treated animals. In contrast, it did not alter sucrose intake in the saline-injected group (Fig. 6j and Extended Data Fig. 10a,b). In addition, animals injected with the inhibitory DREADD and receiving intra-VTA aCSF, or animals injected with control virus and intra-VTA CNO, showed persistent pain-induced decreases in sucrose intake as expected (Fig. 6j and Extended Data Fig. 10c). Interestingly, while inhibition of RMTg–VTA GABAergic input restored the hedonic state of animals in the pain condition, it did not alter CFA-induced hyperalgesia (Fig. 6k). This result demonstrates the role of this pathway in mediating the affective component of pain.

Taken together, these findings show that pain induces an increased inhibitory drive from RMTg GABA neurons onto VTA DA neurons, and that this increase in inhibition is necessary and sufficient to drive anhedonia-like behavior.

## Discussion

Pain triggers maladaptive changes within the mesolimbic reward pathway that can lead to the development of negative affective states[17–19]. Within this pathway, pain impairs MOR-mediated inhibition of GABA release in the VTA[17]. Moreover, inflammatory and neuropathic pain strongly alter opioid-evoked DA release in the NAc[17,18], and alterations in the subpopulations of VTA DA neuron firing properties in a neuropathic pain model have also been reported[36]. However, direct evidence for an effect of pain on VTA DA cell activity and excitability, and its role in mediating changes seen in motivated behavior, has been lacking.

Here, we reported that the RMP of VTA DA neurons is decreased and the rheobase is increased by pain, thereby revealing that DA neurons are less responsive during pain. We demonstrated that the decrease in the intrinsic excitability of VTA DA cells is at least in part mediated by GABAergic inputs providing higher inhibitory drive onto VTA DA neurons. Together with our previous studies[17], these findings suggest that pain downregulates the MOR system at GABA terminals in the VTA, which in turn lead to an increased inhibitory drive and, consequently, a decreased excitability of VTA DA neurons. We also found a non-significant trend toward reduced spontaneous firing rates and input resistance in pain. The lack of a statistically significant effect of pain on spontaneous firing rates could be explained by the increased variability in the datasets, which is suggestive of potentially divergent effects of pain on subpopulations of VTA DA neurons, as previously reported in a different pain model[36]. There is also long-range GABAergic modulation of reward seeking in the NAc, which suggests that local VTA GABA and DA signaling may interact with downstream accumbal modulation of other transmitter systems like acetylcholine, which may be altered

**Fig. 6 | RMTg GABAergic neuronal projections have higher release probability in CFA-treated animals. a**, Schematic (top) and representative image (bottom) of viral injection in the RMTg and recording electrode (indicated by the red dashed circle) in the VTA of GAD-Cre animals. **b**, Representative traces of evoked IPSCs in control (saline) and pain (CFA) condition represented as the mean ± s.e.m. **c**, The PPR is persistently depressed in the condition of pain, which is consistent with a higher release probability (two-way ANOVA for repeated measures; inter-pulse interval: $F_{3,141} = 12.32$, $P < 0.0001$; interaction (inter-pulse interval × treatment): $F_{3,141} = 2.479$, $P = 0.0637$; Dunnett's multiple comparisons post hoc test comparing the PPR at each inter-pulse interval to the baseline: SAL, *$P = 0.0363$; CFA, **$P = 0.0022$; ***$P = 0.0009$; ****$P < 0.0001$, $n = 24$ cells from 4 rats (SAL) or 25 cells from 3 rats (CFA), data represented as mean ± s.e.m.). **d**, Schematic representation of the behavioral methodology. **e**, Representative coronal section of RMTg Gq DREADD-expressing neurons. Blue, DAPI; red, mCherry (Gq DREADD); green, GAD67 (GABA neurons). **f**, The activation of GABA-containing neurons in the RMTg induces a decrease in the amount of 60% sucrose consumed (open bars, baseline; filled bars, 48 h post CNO) (60% sucrose, two-way ANOVA for repeated measures, time: $F_{1,11} = 4.816$, $P = 0.0506$; interaction (time × treatment): $F_{1,11} = 2.786$, $P = 0.1233$; Sidak's post hoc within group: $hM3Dq_{(n=7)}$ baseline versus 48 h post CNO, *$P = 0.0317$). **g**, The activation of GABA-containing neurons in the RMTg induces a decrease in the amount of 5% sucrose consumed (open bars, baseline; filled bars, 48 h post CNO) (5% sucrose, two-way ANOVA for repeated measures, time: $F_{1,11} = 0.3548$, $P = 0.5635$; interaction (time × treatment): $F_{1,11} = 10.96$, $P = 0.0069$; Sidak's post hoc within group: $hM3Dq_{(n=7)}$ baseline versus 48 h post CNO, *$P = 0.03$). **h**, Schematic representation of the behavioral methodology. **i**, Representative coronal section of RMTg Gi DREADD-expressing neurons. Blue, DAPI; red, mCherry (Gi DREADD); green, GAD67 (GABA neurons). **j**, The inhibition of the RMTg–VTA GABAergic pathway restores sucrose consumption in CFA-treated animals (open bars, baseline; filled bars, 48 h (CNO) and 72 h (VEH) post CFA) (two-way ANOVA for repeated measures, time: $F_{2,40} = 28.60$, $P < 0.0001$; interaction (time × treatment): $F_{4,40} = 6.707$, $P = 0.0003$; Sidak's post hoc within group: $hM3Di + CFA\ baseline_{(n=8)}$ versus $hM3Di + CFA + VEH_{(n=8)}$, ****$P < 0.0001$; $hM3Di + CFA + CNO_{(n=8)}$ versus $hM3Di + CFA + VEH_{(n=8)}$, ***$P = 0.0002$; $mCherry + CFA\ baseline_{(n=8)}$ versus $mCherry + CFA + CNO_{(n=8)}$, ****$P < 0.0001$; $mCherry + CFA\ baseline_{(n=8)}$ versus $mCherry + CFA + VEH_{(n=8)}$, ****$P < 0.0001$). **k**, The inhibition of the RMTg–VTA GABAergic pathway does not alter CFA-induced hyperalgesia (schematic on top left) (two-way ANOVA for repeated measures, time: $F_{2,40} = 53.58$, $P < 0.0001$; interaction (time × treatment): $F_{4,40} = 13.19$, $P < 0.0001$; Sidak's post hoc for each group as compared to the group's baseline session: ****$P < 0.0001$). The data are presented as the mean ± s.e.m.

by pain[37]. Additionally, altered excitatory glutamatergic inputs from the ventrolateral periaqueductal gray could play a role in reducing VTA DA neuron activity in conditions of pain[38]. Thus, pain likely dysregulates not only the DA system but also multiple neurotransmitter systems within the mesolimbic reward pathway to drive negative affective states.

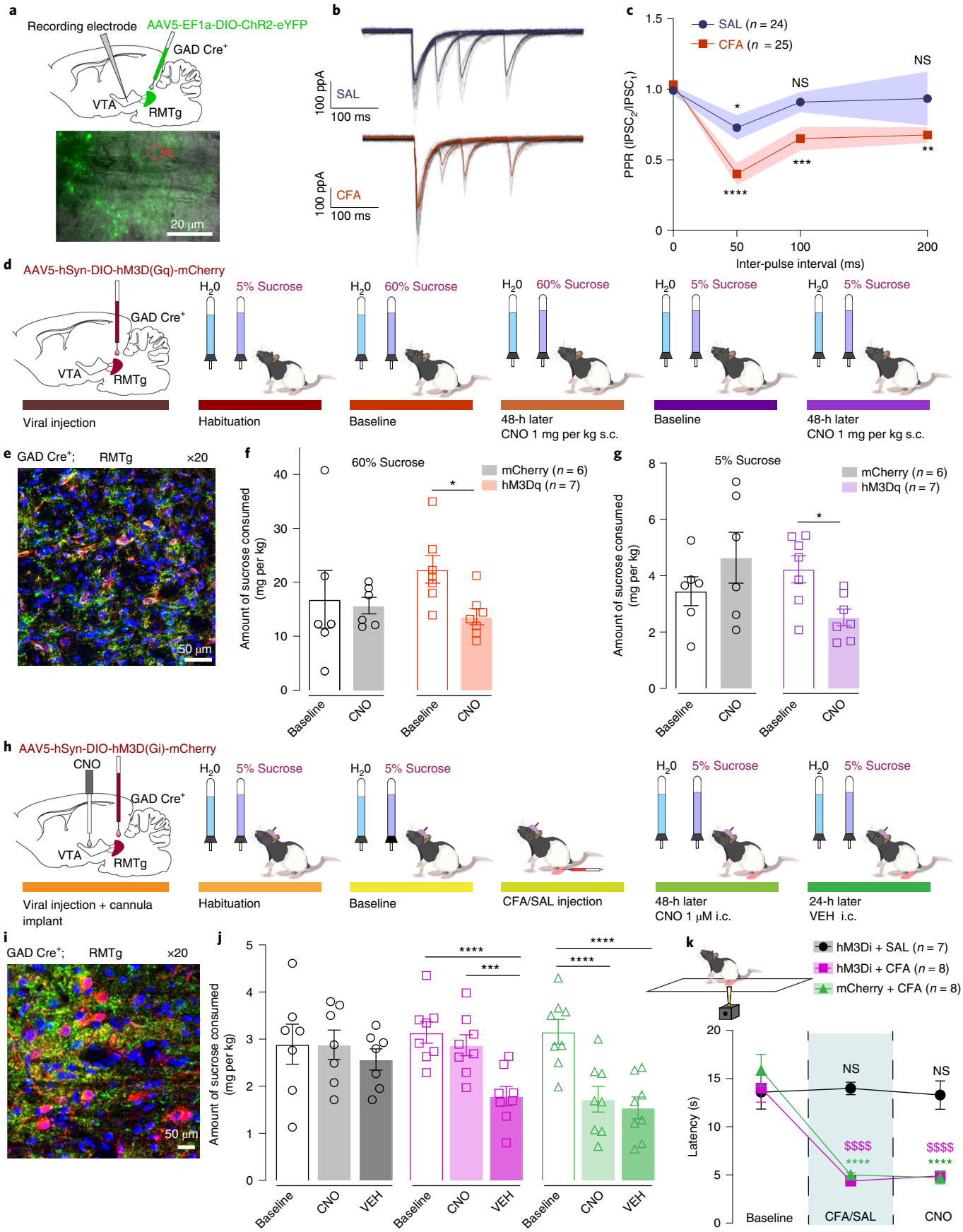

We showed that pain-induced reductions in DA neuron firing are associated with a decreased frequency in VTA DA calcium transients during sucrose self-administration. Interestingly, animals experiencing inflammatory pain showed no significant changes in VTA DA calcium activity during lever presses while seeking the reward, but their phasic DA calcium activity after reward delivery was higher. While this increase in phasic response to reward delivery in pain may be surprising at first, it could be associated with changes in the hedonic state of the animal in pain. Namely, rewards of larger-than-expected value induce a higher phasic response (known as positive reward prediction error)[39,40]. Thus, animals with inflammatory pain experiencing anhedonia may have lower reward expectation and therefore a greater phasic VTA DA response when a reward is received. Our electrophysiology and chemogenetic studies showed that the decreased VTA DA neuron activity is in part due to an increased inhibitory tone from the RMTg. The RMTg plays a critical role in shaping reward prediction error and is inhibited by sucrose or sucrose-predictive cues[35,41]. Thus, it is conceivable that relief from inhibition by RMTg neurons, and the subsequent lower baseline activity of VTA DA neurons, would lead to accentuated phasic changes of VTA DA neuron activity in response to reward delivery.

Chemogenetic activation of VTA DA neurons has been used to demonstrate the role of DA in mediating an increase in motivation for sucrose rewards[28]. Our findings demonstrate that enhancing VTA DA neuron activity or the VTA–NAcSh pathway is sufficient to reverse pain-induced decreases in motivation. While our chemogenetic approach enabled manipulation of a specific pathway, it does not allow for cell-specific activation within that pathway; additional neuronal groups such as GABA- or glutamate-containing neurons may also contribute to this reversal[31,42]. Nevertheless, the number of DREADD-infected DA neurons in the VTA correlated with the percent motivation change in pain, which suggests that this DA population plays a role in the restoration of motivation for sucrose.

The relief of the nociceptive component of ongoing pain is sufficient to produce negative reinforcement through activation of the mesolimbic DA reward pathway[32,43,44]. Our data suggest that activating the DA pathway reverses anhedonia-like behavior but is not sufficient to relieve CFA-induced hyperalgesia. Together, these results suggest that removing the afferent nociceptive information produces negative reinforcement through DA neurotransmission, while activating DA pathways helps resolve the negative emotional components of inflammatory pain.

DA release can be locally modulated at the levels of terminals in the NAc, independently from the DA cell firing; therefore, DA cell firing rate and accumbal DA release may mediate dissociable aspects of DA-related behaviors[45]. While the excitability of DA cells is attenuated in pain, we found that the ex vivo probability of local DA release at the axon terminals in the NAcSh remained unchanged. The lack of a difference in the probability of evoked DA release may also suggest that the pain-induced decrease in motivated behaviors is driven by adaptations at the level of the VTA DA neuron cell body. Although we showed that pain does not affect the properties of DA release at the terminals in the NAc, DA release from NAc terminals is important for motivational deficits in pain states. Specifically, DA release in the NAc induces galanin-receptor-1-triggered depression of excitatory synaptic transmission in the NAc[20] as well as additional adaptations in the dynorphin and enkephalin NAc microcircuitry[19,20,46]. In vivo, chemogenetic stimulation of VTA DA terminals in the NAcSh reversed the pain-induced decrease in motivation without reducing hyperalgesia, which indicates that enhancing the activity of mesolimbic DA neurons can mitigate effects of pain on motivation.

Intake of drugs such as opioids is altered by the presence of pain[17]. Specifically, pain induces a rightward shift in the dose–response curve for opioid self-administration and attenuates opioid-evoked DA release in the NAc[17]. The current findings further contribute to this line of evidence and show that pain decreases the consumption of natural rewards such as sucrose. This effect was overcome if the concentration of sucrose was increased, which suggests that pain induces a dose-dependent shift in the rewarding properties of natural rewards. Importantly, water consumption remained unchanged, which suggests that pain affected the perceived value of the sucrose solution. It has been postulated that the hedonic aspects of both drugs and natural rewards are mediated through opioid systems in the brain[47,48]. In fact, food consumption itself releases endogenous opioids within the mesolimbic pathway[47]. Additionally, pain induces dysfunction of MORs within the VTA, which leads to a decreased motivation to obtain sucrose rewards[17,49]. Our study demonstrated that increasing the concentration of sucrose rewards is sufficient to overcome this effect, possibly by a mechanism that includes enhanced mesolimbic endogenous opioid release[47].

The RMTg provides the main opioid-sensitive inhibitory input onto VTA DA neurons[21,35] and a potential mechanism by which VTA DA neurons are less responsive in pain. We showed that RMTg GABA inputs underlie the reduced excitability of VTA DA neurons in pain. Indeed, enhancing inhibitory drive by chemogenetic activation of RMTg GABA neurons mimicked the effect of pain on sucrose consumption. Interestingly, while pain affected the intake of low- but not high-concentration sucrose rewards, chemogenetic activation of RMTg GABA neurons also decreased the consumption of high-concentration sucrose. One explanation for this finding could be that the chemogenetic approach we employed leads to global activation of RMTg GABA neurons, whereas pain only affects a subset of RMTg GABA neurons, such as those containing MORs[17,22]. Conversely, inhibition of RMTg GABAergic projections to the VTA was sufficient to prevent pain-induced decrease in sucrose consumption without altering sucrose consumption in saline-treated animals. This result demonstrates that the RMTg GABAergic inputs onto VTA are necessary mediators of pain-induced anhedonia-like behavior.

In conclusion, our results provide insight into the regulation of the mesolimbic DA pathway by pain and its consequences on anhedonia-like behaviors. It is important to note that the observed decrease in motivation arises at the initial stages of inflammatory pain and is one of the first symptoms of pain-induced negative affect. As such, further adaptations in the VTA DA circuits could additionally contribute to the development of pain-induced depressive-like behaviors that may arise at later time points in persistent pain[50]. We propose that changes in the VTA DA pathways serve as a potential driver for alterations in circuits mediating those behaviors. The present study uncovered adaptations in a mesolimbic system necessary for the affective component of pain. Our findings increase our understanding of the neural circuitry underlying pain-induced negative affect and provide important mechanistic insight that may contribute to treatments for patients suffering from pain conditions.

## Online content

Any methods, additional references, Nature Research reporting summaries, source data, extended data, supplementary information, acknowledgements, peer review information; details of author contributions and competing interests; and statements of data and code availability are available at https://doi.org/10.1038/s41593-021-00924-3.

Received: 24 January 2020; Accepted: 17 August 2021;
Published online: 18 October 2021

## References

1. Leknes, S. & Tracey, I. A common neurobiology for pain and pleasure. *Nat. Rev. Neurosci.* **9**, 314–320 (2008).

2. Bair, M. J., Robinson, R. L., Katon, W. & Kroenke, K. Depression and pain comorbidity: a literature review. *Arch. Intern. Med.* **163**, 2433–2445 (2003).
3. McWilliams, L. A., Goodwin, R. D. & Cox, B. J. Depression and anxiety associated with three pain conditions: results from a nationally representative sample. *Pain* **111**, 77–83 (2004).
4. Campbell, L. C., Clauw, D. J. & Keefe, F. J. Persistent pain and depression: a biopsychosocial perspective. *Biol. Psychiatry* **54**, 399–409 (2003).
5. Volkow, N. D. & McLellan, A. T. Opioid abuse in chronic pain—misconceptions and mitigation strategies. *N. Engl. J. Med.* **374**, 1253–1263 (2016).
6. Apkarian, A. V. et al. Chronic pain patients are impaired on an emotional decision-making task. *Pain* **108**, 129–136 (2004).
7. Verdejo-García, A., López-Torrecillas, F., Calandre, E. P., Delgado-Rodríguez, A. & Bechara, A. Executive function and decision-making in women with fibromyalgia. *Arch. Clin. Neuropsychol.* **24**, 113–122 (2009).
8. Wiech, K. et al. Influence of prior information on pain involves biased perceptual decision-making. *Curr. Biol.* **24**, R679–R681 (2014).
9. Seixas, D., Palace, J. & Tracey, I. Chronic pain disrupts the reward circuitry in multiple sclerosis. *Eur. J. Neurosci.* **44**, 1928–1934 (2016).
10. Nestler, E. J. & Carlezon, W. A. The mesolimbic dopamine reward circuit in depression. *Biol. Psychiatry* **59**, 1151–1159 (2006).
11. Schultz, W. Behavioral dopamine signals. *Trends Neurosci.* **30**, 203–210 (2007).
12. Berridge, K. C. & Robinson, T. E. What is the role of dopamine in reward: hedonic impact, reward learning, or incentive salience? *Brain Res. Rev.* **28**, 309–369 (1998).
13. Bromberg-Martin, E. S., Matsumoto, M. & Hikosaka, O. Dopamine in motivational control: rewarding, aversive, and alerting. *Neuron* **68**, 815–834 (2010).
14. Martikainen, I. K. et al. Chronic back pain is associated with alterations in dopamine neurotransmission in the ventral striatum. *J. Neurosci.* **35**, 9957–9965 (2015).
15. Scott, D. J., Heitzeg, M. M., Koeppe, R. A., Stohler, C. S. & Zubieta, J.-K. Variations in the human pain stress experience mediated by ventral and dorsal basal ganglia dopamine activity. *J. Neurosci.* **26**, 10789–10795 (2006).
16. Benarroch, E. E. Involvement of the nucleus accumbens and dopamine system in chronic pain. *Neurology* **87**, 1720–1726 (2016).
17. Hipolito, L. et al. Inflammatory pain promotes increased opioid self-administration: role of dysregulated ventral tegmental area opioid receptors. *J. Neurosci.* **35**, 12217–12231 (2015).
18. Taylor, A. M. W. et al. Microglia disrupt mesolimbic reward circuitry in chronic pain. *J. Neurosci.* **35**, 8442–8450 (2015).
19. Massaly, N. et al. Pain-induced negative affect is mediated via recruitment of the nucleus accumbens kappa opioid system. *Neuron* **102**, 564–573.e6 (2019).
20. Schwartz, N. et al. Decreased motivation during chronic pain requires long-term depression in the nucleus accumbens. *Science* **345**, 535–542 (2014).
21. Matsui, A., Jarvie, B. C., Robinson, B. G., Hentges, S. T. & Williams, J. T. Separate GABA afferents to dopamine neurons mediate acute action of opioids, development of tolerance and expression of withdrawal. *Neuron* **82**, 1346–1356 (2014).
22. Ozaki, S. et al. Suppression of the morphine-induced rewarding effect in the rat with neuropathic pain: implication of the reduction in μ-opioid receptor functions in the ventral tegmental area. *J. Neurochem.* **82**, 1192–1198 (2002).
23. Hodos, W. Progressive ratio as a measure of reward strength. *Science* **134**, 943–944 (1961).
24. Brennan, K., Roberts, D. C., Anisman, H. & Merali, Z. Individual differences in sucrose consumption in the rat: motivational and neurochemical correlates of hedonia. *Psychopharmacology (Berl.)* **157**, 269–276 (2001).
25. Kitai, S. T., Shepard, P. D., Callaway, J. C. & Scroggs, R. Afferent modulation of dopamine neuron firing patterns. *Curr. Opin. Neurobiol.* **9**, 690–697 (1999).
26. Neuhoff, H., Neu, A., Liss, B. & Roeper, J. $I_h$ channels contribute to the different functional properties of identified dopaminergic subpopulations in the midbrain. *J. Neurosci.* **22**, 1290–1302 (2002).
27. Saddoris, M. P., Cacciapaglia, F., Wightman, R. M. & Carelli, R. M. Differential dopamine release dynamics in the nucleus accumbens core and shell reveal complementary signals for error prediction and incentive motivation. *J. Neurosci.* **35**, 11572–11582 (2015).
28. Boekhoudt, L. et al. Enhancing excitability of dopamine neurons promotes motivational behaviour through increased action initiation. *Eur. Neuropsychopharmacol.* **28**, 171–184 (2018).
29. Yang, H. et al. Nucleus accumbens subnuclei regulate motivated behavior via direct inhibition and disinhibition of VTA dopamine subpopulations. *Neuron* **97**, 434–449.e4 (2018).
30. Al-Hasani, R. et al. Distinct subpopulations of nucleus accumbens dynorphin neurons drive aversion and reward. *Neuron* **87**, 1063–1077 (2015).
31. Boender, A. J. et al. Combined use of the canine adenovirus-2 and DREADD-technology to activate specific neural pathways in vivo. *PLoS ONE* **9**, e95392 (2014).
32. Navratilova, E. et al. Pain relief produces negative reinforcement through activation of mesolimbic reward–valuation circuitry. *Proc. Natl Acad. Sci. USA* **109**, 20709–20713 (2012).
33. Liu, M.-Y. et al. Sucrose preference test for measurement of stress-induced anhedonia in mice. *Nat. Protoc.* **13**, 1686–1698 (2018).
34. van Zessen, R., Phillips, J. L., Budygin, E. A. & Stuber, G. D. Activation of VTA GABA neurons disrupts reward consumption. *Neuron* **73**, 1184–1194 (2012).
35. Jhou, T. C., Fields, H. L., Baxter, M. G., Saper, C. B. & Holland, P. C. The rostromedial tegmental nucleus (RMTg), a GABAergic afferent to midbrain dopamine neurons, encodes aversive stimuli and inhibits motor responses. *Neuron* **61**, 786–800 (2009).
36. Huang, S., Borgland, S. L. & Zamponi, G. W. Peripheral nerve injury-induced alterations in VTA neuron firing properties. *Mol. Brain* **12**, 89 (2019).
37. Creed, M. C., Ntamati, N. R. & Tan, K. R. VTA GABA neurons modulate specific learning behaviors through the control of dopamine and cholinergic systems. *Front. Behav. Neurosci.* **8**, 8 (2014).
38. Waung, M. W., Margolis, E. B., Charbit, A. R. & Fields, H. L. A midbrain circuit that mediates headache aversiveness in rats. *Cell Rep.* **28**, 2739–2747.e4 (2019).
39. Schultz, W. Dopamine reward prediction error coding. *Dialogues Clin. Neurosci.* **18**, 23–32 (2016).
40. Schultz, W., Dayan, P. & Montague, P. R. A neural substrate of prediction and reward. *Science* **275**, 1593–1599 (1997).
41. Li, H. et al. Three rostromedial tegmental afferents drive triply dissociable aspects of punishment learning and aversive valence encoding. *Neuron* **104**, 987–999.e4 (2019).
42. Morales, M. & Margolis, E. B. Ventral tegmental area: cellular heterogeneity, connectivity and behaviour. *Nat. Rev. Neurosci.* **18**, 73–85 (2017).
43. Navratilova, E. & Porreca, F. Reward and motivation in pain and pain relief. *Nat. Neurosci.* **17**, 1304–1312 (2014).
44. Leknes, S., Lee, M., Berna, C., Andersson, J. & Tracey, I. Relief as a reward: hedonic and neural responses to safety from pain. *PLoS ONE* **6**, e17870 (2011).
45. Mohebi, A. et al. Dissociable dopamine dynamics for learning and motivation. *Nature* **570**, 65–70 (2019).
46. Liu, S. et al. Neuropathic pain alters reward and affect via kappa opioid receptor (KOR) upregulation. *FASEB J.* https://doi.org/10.1096/fasebj.30.1_supplement.928.5 (2016).
47. Hayward, M. D., Schaich-Borg, A., Pintar, J. E. & Low, M. J. Differential involvement of endogenous opioids in sucrose consumption and food reinforcement. *Pharmacol. Biochem. Behav.* **85**, 601–611 (2006).
48. Nummenmaa, L. et al. μ-opioid receptor system mediates reward processing in humans. *Nat. Commun.* **9**, 1500 (2018).
49. Harris, R. E. et al. Decreased central μ-opioid receptor availability in fibromyalgia. *J. Neurosci.* **27**, 10000–10006 (2007).
50. Zhou, W. et al. A neural circuit for comorbid depressive symptoms in chronic pain. *Nat. Neurosci.* https://doi.org/10.1038/s41593-019-0468-2 (2019).

## Methods

**Animals.** All procedures were approved by Washington University and the National Institute on Alcohol Abuse and Alcoholism (NIAAA) Animal Care and Use Committee in accordance with the National Institutes of Health Guidelines for the Care and Use of Laboratory Animals.

Adult male and female Long Evans wild-type, TH-Cre and GAD-Cre rats (250–350 g), and adult male and female $DAT^{IRES\text{-}Cre}$ mice crossed with Cre-driven expression of ChR2 mice (AiCop4) were used for this study. All animals for behavioral experiments were 8–10 weeks old at the beginning of the experiments. Animals used for patch-clamp electrophysiology were between 3.5 and 6 weeks old (for optogenetic studies). Rats were group-housed with two to three animals per cage on a 12/12-h dark/light cycle (lights on at 7:00) and acclimated to the animal facility holding rooms for at least 7 days before any manipulation. Mice were housed up to four animals per cage. The temperature for the holding rooms of all animals ranged from 21 to 24 °C while the humidity was between 30 and 70%.

All experiments were performed during the light cycle. Rats received food and water ad libitum until 2 days before starting the behavioral studies, when food restriction (16 g of rat chow per day) started and continued until the end of the experiments. Mice received food and water ad libitum throughout the entire experimental procedure.

**Surgeries.** All surgeries were performed under isoflurane (2.5/3 minimum alveolar concentration) anesthesia using appropriate sterile aseptic techniques.

*Intracerebral injections.* For chemogenetic activation of VTA DA neurons and fiber photometry recordings of VTA DA neuron activity, TH-Cre rats were bilaterally injected with AAV5-hSyn-DIO-hM3D(Gq)-mCherry, AAV5-Ef1a-DIO-mCherry or AAV-DJ-EF1a-DIO-GCaMP6s (all viruses injected at $1.5–2.5 \times 10^{12}$ transducing units per ml (0.5 µl per side), Addgene), and/or implanted with a fiber optic (Doric Lenses) in the VTA (stereotaxic coordinates for viral injections from Bregma: anterior–posterior (AP) = -5.3 mm, medial–lateral (ML) = ±0.7 mm, dorsal–ventral (DV) = −8 mm; stereotaxic coordinates for optic fiber from Bregma: AP = −5.3 mm, ML = ±0.7 mm, DV = −7.8 mm from the skull surface, World Precision Instruments). The optic fiber implant was secured to the skull using three sterile bone screws and a dental cement head-cap (Lang Dental).

For chemogenetic activation of NAc-projecting VTA DA terminals in addition to DREADD injections, animals received bilateral intra-NAc cannula implants (stereotaxic coordinates for cannula implant from Bregma: AP = +1.2 mm, ML = −0.8 mm, DV = −6.0 mm from the skull surface, with injectors extending 1 mm past the tip of the cannula) for the local delivery of either aCSF or CNO.

For chemogenetic activation of RMTg GABA neurons, GAD-Cre rats were bilaterally injected with either AAV5-hSyn-DIO-hM3D(Gq)-mCherry or AAV5-Ef1a-DIO-mCherry ($1.5–2.5 \times 10^{12}$ transducing units per ml (0.5 µl per side), Addgene) in the RMTg (stereotaxic coordinates from Bregma: AP = −6.8 mm, ML = ±1.6 mm, DV = −8.4 mm from skull surface under 10° angle).

For chemogenetic inhibition of RMTg-VTA GABA neurons, GAD-Cre rats were bilaterally injected with either AAV5-hSyn-DIO-hM3D(Gi)-mCherry or AAV5-Ef1a-DIO-mCherry ($2.5–2.9 \times 10^{12}$ transducing units per ml (0.5 µl per side), Addgene) in the RMTg (stereotaxic coordinates from Bregma: AP = −6.8 mm, ML = ±1.6 mm, DV = −8.4 mm from skull surface under 10° angle). At the same time, animals were bilaterally implanted with intra-VTA cannula implants (stereotaxic coordinates for cannula implant from Bregma: AP = −5.3 mm, ML = ±0.7 mm, DV = −7 mm from the skull surface, with injectors extending 1 mm past the tip of the cannula) for the local delivery of either aCSF or CNO.

For the combined chemogenetics experiments, wild-type rats were bilaterally injected with retrograde canine adenovirus CAV2-Cre ($2.14 \times 10^{12}$ transducing units per ml (0.5 µl per side), The Institute of Molecular Genetics of Montpellier) in the NAc (stereotaxic coordinates for viral injections from Bregma: AP = +1.2 mm, ML = −0.8 mm, DV = −7.0 mm from the skull surface) and either AAV5-hSyn-DIO-hM3D(Gq)-mCherry or AAV5-Ef1a-DIO-mCherry in the VTA. Following viral injections, the incision was closed using sterile stainless steel wound clips (Autoclip, Braintree Scientific).

For optogenetic electrophysiology recordings, 4-week old GAD-Cre rats were injected bilaterally with AAV5-EF1a-DIO-ChR2-eYFP in the RMTg (stereotaxic coordinates for viral injections from Bregma: AP = −6.3 mm, ML = ±1.4 mm, DV = −7.4 mm from skull surface under 10° angle).

To avoid post-surgical complications and to minimize pain, animals received a daily s.c. injection of 8 mg per kg enrofloxacin and 5 mg per kg carprofen solution for 2 consecutive days together with complementary carprofen chewable tablets. Behavioral experiments were started either 3 or 5 weeks after intracerebral injections to allow for maximal viral expression at the time of testing.

*CFA injections.* Animals were sedated using isoflurane anesthesia. Once appropriate sedation was achieved, as determined by the lack of reflex during toe-pinch, rats and mice were injected in the right hindpaw with 200 µl or 50 µl, respectively, of CFA solution (Thermo Fisher). Saline-injected animals served as controls. The general behavior (feeding, drinking and locomotion) of the animals was monitored throughout the duration of experiments.

**Ex vivo FSCV.** Mice were anesthetized with isoflurane and euthanized by decapitation. Brains were sliced in sagittal orientation at 240-µm thickness with a vibratome (VT-1200S Leica) in an ice-cold cutting solution containing the following (in mM): 225 sucrose, 13.9 NaCl, 26.2 $NaHCO_3$, 1 $NaH_2PO_4$, 1.25 glucose, 2.5 KCl, 0.1 $CaCl_2$, 4.9 $MgCl_2$ and 3 kynurenic acid. Slices were incubated for 20 min at 33 °C in aCSF containing (in mM) 124 NaCl, 1 $NaH_2PO_4$, 2.5 KCl, 1.3 $MgCl_2$, 2.5 $CaCl_2$, 20 glucose, 26.2 $NaHCO_3$ and 0.4 ascorbic acid, and maintained at room temperature before recordings. Slices were placed in a submerged chamber perfused at 2 ml $min^{-1}$ with aCSF at 32 °C using an in-line heater (Harvard Apparatus). Cylindrical carbon-fiber electrodes (CFEs) were prepared with T650 fibers (6 µm in diameter, ~150 µm of exposed fiber) inserted into a glass pipette. Before use, the CFEs were conditioned with a 8-ms-long triangular voltage ramp (−0.4 to +1.2 and back to −0.4 V versus an Ag/AgCl reference at 4 V $s^{-1}$) delivered every 15 ms. CFEs showing current above 1.8 µA or below 1.0 µA in response to the voltage ramp around 0.6 V were discarded.

DA transients were recorded using the same triangular voltage ramp delivered every 100 ms in the NAcSh area (AP: +1.30 mm, ML: ±0.5 mm, DV: −4.75 mm), and evoked by either monopolar electrical stimulation through an aCSF-filled glass pipette placed by passing a rectangular pulse of 100–250 µA of 0.2 ms in duration (Cygnus Technology) or a brief light pulse (1 or 2 ms) via an optical fiber (200 µm/0.22 NA) connected to a 470-nm light-emitting diode (LED; 2 mW; ThorLabs) delivered every 2 min. Data were collected with a modified electrochemical headstage (CB-7B/EC retrofit with a 5 MΩ resistor) using a Multiclamp 700B amplifier (Molecular Devices) after being low-pass-filtered at 10 kHz and digitized at 100 kHz using custom-written software in Igor Pro 7 (v.7.0.6.1, Wavemetrics) running mafPC 2019 software (courtesy of M. A. Xu-Friedman, University at Buffalo). Custom-written analysis software in Igor Pro was used for analysis. Decay time constants were obtained with a single exponential fit of the derivative of the falling phase of the DA transient curve.

**Patch-clamp electrophysiology.** Patch-clamp electrophysiology data acquisition was completed using Clampex 11.4 software (Molecular Devices). Visualized whole-cell recording techniques were used to measure the holding and synaptic responses of DA neurons in the VTA. Currents were amplified, low-pass-filtered at 4 kHz and digitized at 10 kHz. Recordings were performed in whole-cell configuration with patch pipette internal solution containing the following (in mM): 130 potassium gluconate, 10 phosphocreatine disodium salt, 4 $MgCl_2$, 3.4 $Na_2ATP$, 0.1 $Na_3GTP$, 1.1 EGTA and 5 HEPES. All recordings were performed in DA neurons identified by (1) a cellular capacitance >30 pF, (2) a spontaneous firing below 5 Hz and (3) the presence of a large hyperpolarization-activated inward current, $I_h$. To ascertain the presence of $I_h$ currents, neurons were voltage-clamped at −60 mV, and the response to five hyperpolarizing voltage steps (250 ms, −25 to −125 mV in increments of −25 pA) were measured. The spontaneous activity and the responses to current injections were made in current-clamp configuration. Spontaneous firing rates and RMPs were recorded for 5 min in 5 trials of 60 s. To generate an input–output curve of neuronal excitability, 200-ms current steps were injected in increments of 10 pA from −50 to 200 pA, and the numbers of spikes were quantified for each step. Rheobase values were determined by injecting 100-ms ramps of increasing current (0–180 pA) and measuring the current where the first action potential was observed. To assess the impact of inhibition on DA neuron excitability, experiments were first conducted in the presence of the glutamate receptor antagonist kynurenic acid (2 mM) and again after aCSF containing the $GABA_A$ receptor antagonist PTX (100 µM) was washed on. Spontaneous IPSCs were recorded in the presence of kynurenic acid (2 mM). VTA DA neurons were voltage-clamped at −60 mV with patch pipette internal solution containing (in mM) 100 KCl, 30 potassium gluconate, 4 $MgCl_2$, 10 phosphocreatine disodium salt, 3.4 $Na_2ATP$, 0.1 $Na_3GTP$, 1.1 EGTA and 5 HEPES. Recordings were excluded if the series resistance or noise level varied by more than 25% over the course of recordings.

To record RMTg-evoked IPSCs onto VTA DA neurons, VTA slices were prepared 2 weeks following viral injection of channelrhodopsin (ChR2) into the RMTg of GAD-Cre rats. VTA DA neurons were voltage-clamped at −60 mV with patch pipette internal solution containing (in mM) 100 KCl, 30 potassium gluconate, 4 $MgCl_2$, 10 phosphocreatine disodium salt, 3.4 $Na_2ATP$, 0.1 $Na_3GTP$, 1.1 EGTA and 5 HEPES. Activation of ChR2-expressing RMTg terminals was accomplished by a LED mounted in the epifluorescence light path. Light power was modulated to the lowest intensity at which we could consistently evoke a post-synaptic response, up to a maximum of 15 mW. IPSCs were isolated by the addition of the glutamate receptor antagonist kynurenic acid (2 mM) to the aCSF. Responses to paired stimuli were assessed at interleaved inter-stimulus intervals of 50, 100 and 200 ms. The PPR was calculated as the amplitude ratio $IPSC_2/IPSC_1$.

Recordings from saline-treated and CFA-treated pairs of rats were interleaved within each day.

**Operant conditioning.** Sucrose self-administration by rats was conducted using operant-conditioning chambers (Med Associates, MED, PC 5 software) equipped with two retractable levers positioned on the right-hand wall and a food magazine connected to a food pellet dispenser between them. Two cue lights were positioned above the levers, and one house light was positioned on the top left-hand wall.

During the self-administration sessions, both levers (active and inactive) were extended out with the white cue light turned on only above the active lever. Presses on the active lever resulted in sucrose pellet delivery and a 20-s time-out period during which the active and inactive levers were retracted, and the cue light above the active lever was turned off. Presses on the inactive lever did not result in any changes in the environment.

Three to five weeks after the surgical procedure (chemogenetic activation of VTA DA neurons, chemogenetic activation of the VTA–NAc pathway and photometry), animals were trained to self-administer sucrose pellets as follows. First, animals were placed in operant boxes under the FR1 schedule of reinforcement for sucrose self-administration for 2 h or until the rat reached a maximum of 60 rewards. Once the animals completed 3 consecutive daily sessions obtaining 60 rewards, they were then exposed to 3 FR2 sessions followed by 3 FR5 sessions. On the following day, animals were gently placed back in the self-administration enclosures and were given access to sucrose during a 2-h session on a PR schedule of reinforcement, during which the number of correct lever presses to receive the following reward increases exponentially ($5 \times e^{(0.2 \times \text{infusion number})} - 5$ rounded to the nearest integer resulting in the following PR steps: 1, 2, 6, 9, 12, 15, 20, 25, 32, 40, 50, 62, 77, 95…. Following the baseline PR session, animals received an injection of either saline or CFA in the right hindpaw. Forty-eight hours after inflammatory pain induction, rats underwent a second 2-h PR session. For chemogenetic activation of VTA DA neurons, or the VTA–NAc pathway, CNO (1 mg per kg s.c., Sigma) was administered 20 min before starting the second PR session.

For chemogenetic activation of VTA–NAcSh-projecting DA terminals, 250 µl per side intra-NAcSh microinjections of aCSF (on PR1), and aCSF or 1 mM CNO (on PR2) were delivered over 5 min using Harvard Pump 11 Elite Series. Injectors were left in place for an additional 2.5 min to allow for diffusion of the injected solution. Fifteen minutes after the start of the intra-NAcSh injection, animals were placed in the boxes and PR sessions were started.

**Open-field test for locomotor activity.** Open-field tests were performed in square enclosures (60 × 60 cm) within a sound-attenuated room at 23 °C room temperature. Animals underwent three 5-min habituation sessions followed by a 30-min baseline session. Following the baseline session, animals received either CFA or saline injections in the paw. Forty-eight hours after the intraplanar injections, s.c. injections of either CNO (1 mg per kg) or saline were administered. Second, a 30-min testing session in the open field started 20 min after the s.c. injections. At the beginning of each session, animals were placed in the center of the open field and the total distance traveled was recorded and analyzed using AnyMaze 6.06 (64-bit) behavioral tracking software (Stoelting).

**Hargreaves plantar test for thermal sensitivity.** To assess thermal hyperalgesia induced by CFA injection, we used the Hargreaves plantar test (IITC Life Science). Animals were placed in Plexiglass boxes on top of a glass surface. After 15 min of habituation, a heat source was applied on the plantar surface of the right hindpaw, and the latency of paw withdrawal from the heat stimulus was recorded. Animals underwent three habituation sessions before testing. Testing sessions consisted of four measurements with at least a 5-min interval between trials. Latency was determined by averaging all four trials per each testing session.

For chemogenetic experiments, thermal hyperalgesia was assessed 1 h before the PR1 (baseline) and PR2 (CFA/saline) sessions. To investigate the sufficiency of chemogenetic activation/silencing of the neuronal pathway in hyperalgesic states during PR tests, an additional Hargreaves session was performed on the day following PR2 session 20 min after saline or CNO s.c. injection, or 15 min after aCSF or CNO intra-NAcSh microinjections.

For locomotor experiments, thermal hyperalgesia was assessed 1 h before baseline and testing (CFA/saline) sessions. An additional Hargreaves session was performed on the day following locomotor testing session 20 min after saline or CNO s.c. injection to ensure that chemogenetic activation of VTA DA neurons does not alter CFA-induced hyperalgesia in these animals.

For photometry studies, thermal hyperalgesia was tested 1 h before any PR sessions.

Last, for the two-bottle choice experiments (see below), thermal hyperalgesia was assessed 1 h before baseline and post-CFA/saline and post-CNO testing sessions.

**Orofacial reactivity.** Animals were water restricted as for the two-bottle choice experiment. Rats were individually placed in a cage with no bedding and free access to a solution (water or 5%, 30% or 60% sucrose) placed in a Petri dish on the floor. Rats were filmed at 100 frames per second during drinking bouts. Consummatory and hedonic tongue protrusions from the three first bouts were scored offline. Hedonic protrusions were defined as any event where the tongue was extended out of the mouth but did not contact the sucrose solution, in contrast to consummatory protrusions. For each rat, only one solution was tested per day and the order of solutions was counterbalanced within rats. In a separate session, rats were given free access to 0.05% quinine and aversive gapes were scored.

**Two-bottle choice.** For the two-bottle choice studies, animals were water-restricted to 4 h of water access following the experimental session. For testing sessions, rats were individually placed in a cage with no bedding and free access to either water or sucrose solutions placed on top of the wire rack covering the cage. Placement of the water and sucrose solution bottles (right or left) was counterbalanced. After four daily 1-h habituation sessions during which animals were exposed to water and a 5% sucrose solution, a baseline measurement of water and sucrose (5%, 30% or 60%) consumption was obtained. Immediately after the baseline session, CFA was injected in the hindpaw of the animal as described above. Saline injection was used as a control. Forty-eight hours after intraplantar injection, another test was conducted to determine the impact of pain on water and sucrose solution consumption.

For chemogenetic studies, CNO (1 mg per kg s.c.) was injected 20 min, or 5 min for intracranial CNO 1 mM injection, before starting a two-bottle choice testing session. All measurements for water and sucrose consumption were recorded as the volume (ml) and amount (g) of liquid consumed using a weighing scale.

**Immunohistochemistry.** Following each behavioral experiment, rats were transcardially perfused with PBS followed by 4% paraformaldehyde. For the cFos experiments, rats were perfused for 90 min following the s.c. injection of either 1 mg per kg CNO or saline to allow for maximal neuronal activation. Brains were collected and kept at 4 °C for 24 h in 4% paraformaldehyde for post-fixation, followed by 72 h incubation in 30% sucrose solution. Isopentane was used to flash-freeze brain tissue, which was consequently cut in 40-µm coronal slices using a cryostat (Leica CM 1950). Free-floating sections containing the VTA were washed in PBS and blocked with normal donkey serum (Millipore, S30) and 0.3% Triton–0.01 M PBS (PBS-T) and incubated overnight in 3% normal donkey serum and 0.3% PBS-T containing TH (1:2,000; mouse anti-TH, MAB318, Millipore), mCherry (1:500; rabbit anti-mCherry, ab167453, Abcam; or chicken anti-mCherry for cFos experiments and VTA cannula verification, ab205402 Abcam) and/or cFos (1:2,000; rabbit anti-cFos, ab190289, Abcam). The following day, sections were again rinsed with PBS and then incubated (2 h) with the appropriate secondary antibodies diluted in 3% normal donkey serum and 0.3% PBS-T (for TH donkey anti-mouse A488; for mCherry in cFos experiments and cannula verification donkey anti-chicken Cy3 or donkey anti-rabbit Cy3 for all other experiments; for cFos donkey anti-rabbit DyLight405). All secondary antibodies were diluted 1:200 and were from Jackson ImmunoResearch.

In GAD-Cre rats, brain sections containing the RMTg were processed for GAD67 immunoreactivity. Briefly, sections were washed and blocked as described above and incubated overnight in GAD67 (1:5,000; mouse anti-GAD67, MAB5406, EMDMillipore). The following day, sections underwent a series of steps for tyramide signal amplification (TSA; 1 h streptavidin–horseradish peroxidase, 15 min TSA–biotin using a TSA kit (Perkin Elmer). Sections were rinsed and then incubated with streptavidin AF488 (1:200; Jackson ImmunoResearch).

A Leica DMR microscope was used to process images (×5, ×10 and/or ×20 magnification) of viral expression. ImageJ 1.53a software was used to manually quantify the number of labeled cells for combined chemogenetics experiments and cFos activation. For combined chemogenetic quantification, VTA images were taken at ×10 magnification and neuronal counts were performed in all VTA slices expressing mCherry from –4.80 AP to –6.12 AP. For cFos quantification, VTA images were taken at ×20 magnification and 3 VTA slices of equivalent distance from Bregma between –4.80 AP and –6.12 AP were quantified per animal. Cell counts were done by two independent researchers that were blinded to the experimental results and treatments.

**Photometry acquisition.** For fiber photometry studies, rats were food restricted and trained in operant conditioning (Med Associates) as described for the behavioral paradigm above. Fiber photometry recordings were made throughout the entirety of the 2-h PR operant conditioning sessions. Before recording during operant behavior sessions, an optic fiber was attached to the implanted fiber using a ferrule sleeve (Doric, ZR_2.5). Two LEDs were used to excite GCaMP6s. A 531-Hz sinusoidal LED light (Thorlabs, LED light: M470F3; LED driver: DC4104) was bandpass-filtered (470 ± 20 nm, Doric, FMC4) to excite GCaMP6s and evoke $Ca^{2+}$-dependent emission. A 211-Hz sinusoidal LED light (Thorlabs, LED light: M405FP1; LED driver: DC4104) was bandpass-filtered (405 ± 10 nm, Doric, FMC4) to excite GCaMP6s and evoke $Ca^{2+}$-independent isosbestic control emission. Laser intensities for the 470-nm and 405-nm wavelength bands were measured at the tip of the optic fiber and adjusted to 50 µW before each day of recording. GCaMP6s fluorescence traveled through the same optic fiber before being bandpass-filtered (525 ± 25 nm, Doric, FMC4), transduced by a femtowatt silicon photoreceiver (Newport, 2151) and recorded using a real-time processor (TDT, RZ5P). The envelopes of the 531-Hz and 211-Hz signals were extracted in real-time using the TDT program Synapse v.95 at a sampling rate of 1,017.25 Hz.

**Experimental design and statistics.** All the experiments were successfully replicated at least twice, including each treatment condition, to prevent a nonspecific day/condition effect. Treatment groups were randomly assigned to animals before testing. No statistical methods were used to predetermine sample sizes, but our sample sizes were similar to those reported in previous publications[17,19]. After assessing the normality of sample data using D'Agostino and Pearson tests and Shapiro–Wilk tests, statistical significance was taken as

$^{*}P<0.05$, $^{**}P<0.01$, $^{***}P<0.001$ and $^{****}P<0.0001$, as determined by two-way repeated-measures analysis of variance (ANOVA) followed by two-tailed Sidak's post hoc test, Friedman's test, two-tailed unpaired *t*-test, two-tailed paired *t*-test, Kruskal–Wallis test, two-tailed Dunn's multiple comparisons test, two-tailed Wilcoxon test, two-tailed uncorrected Dunn's test, Dunnett's multiple comparisons test, Kolmogorov–Smirnov test, one sample *t*-test or two-tailed Mann–Whitney for unpaired values as appropriate. For correlation analysis between neuronal counts and percent motivation change (Fig. 3i–k), Hartigan dip test was used to test for non-unimodality (permutation number = 20,000), followed by a comparison of medians in a nonparametric way using Wilcoxon rank-sum test. Correlation within the bimodally distributed groups, or all data combined, was performed using Spearman's test. No outliers were excluded from any of the studies presented in this manuscript.

All data are expressed as the mean ± s.e.m. Sample sizes (*n* number) always refer to values obtained from an individual animal in all behavioral experiments (Figs. 1 and 3–6), individual cell recordings (Figs. 2 and 6) or slice analysis (Supplementary Fig. 3). Statistical analyses were performed using GraphPad Prism 8.1.0 and Matlab. Data collection and analysis were performed blinded to the conditions of the experiments.

Custom Matlab scripts were developed for analyzing fiber photometry data in the context of rat behavior. The isosbestic 405-nm excitation control signal was subtracted from the 470-nm excitation signal to remove movement artifacts from intracellular $Ca^{2+}$-dependent GCaMP6s fluorescence. Baseline drift was evident in the signal due to slow photobleaching artifacts, particularly during the first several minutes of each 2-h recording session. A double exponential curve was fit to the raw trace and subtracted to correct for baseline drift. After baseline correction, the photometry trace was normalized to units of $\Delta F/F$ using the median fluorescence of the entire session for subtraction and division. The post-processed fiber photometry signal was analyzed in the context of PR task performance. For equivalent comparisons between baseline and post-CFA PR sessions, analysis of the mean fluorescence relative to lever press times and reward attainment times was restricted to the minimum number of lever presses (first 34 lever presses per session) and rewards (first 6 rewards per session) obtained by an animal within a given session. The transient event rate for individual sessions was determined by identifying local maxima in the $\Delta F/F$ photometry signal that resemble the waveform and temporal dynamics of GCaMP6s calcium transients. The built-in Matlab function findpeaks was used to identify local maxima that were at least 1.2% $\Delta F/F$ in prominence and at least 150 ms in width at half prominence (Supplementary Fig. 1). For quantification of fluorescence during lever pressing, the mean $\Delta F/F$ was calculated −3 to 0 s relative to each lever press. For quantification of fluorescence during reward delivery, the maximum $\Delta F/F$ was calculated 2–5 s relative to reward delivery to account for latency in pellet consumption.

**Reporting Summary.** Further information on research design is available in the Nature Research Reporting Summary linked to this article.

## Data availability

The data that support the findings of this study are available from the corresponding authors upon request.

## Code availability

Custom Matlab scripts generated during and/or analyzed during the current study are publicly available from the following link: https://github.com/christianepedersen. Custom-written analysis software Igor Pro 7 and mafPC is publicly available from the following links: https://bitbucket.org/r-bock/vigor/src/master/, https://bitbucket.org/r-bock/common-igor-functions/src/master/ and https://www.xufriedman.org/mafpc.

## Acknowledgements

We would like to thank all members from the Moron-Concepcion, Bruchas, Creed and Alvarez laboratories for their help throughout the completion of the current study. In addition, we thank I. Monosov for help with statistical analysis for Fig. 3i,j,k, and A. R. Wilson-Poe for manuscript review and editing. This work was supported by US National Institutes of Health (NIH) grants DA041781 (to J.A.M.), DA042581 (to J.A.M.), DA042499 (to J.A.M.), DA041883 (to J.A.M.) and DA045463 (to J.A.M.), a NARSAD Independent Investigator Award from the Brain and Behavior Research Foundation (to J.A.M.), the Brain and Behavior Research Foundation (NARSAD Young Investigator grant 27197 to M.C.C.), National Institutes of Health National Institute on Drug Abuse R21-DA047127 (to M.C.C.) and R01-DA049924 (to M.C.C.), Whitehall Foundation grant 2017-12-54 (to M.C.C.), a Rita Allen Scholar Award in Pain (to M.C.C.), and NRSA F31DA051124 (to C.E.P.).

## Author contributions

Conceptualization: T.M., N.M., C.E.P., J.H.S., V.A.A., M.R.B., M.C.C. and J.A.M. Methodology: T.M., V.A.A., M.R.B., M.C.C. and J.A.M. Formal analysis of all data: T.M., M.C.C. and J.A.M. Photometry acquisition and data extraction: T.M. and C.E.P. Patch-clamp physiology: Y.M.V., C.A.M., K.A. and M.C.C. Operant sucrose self-administration: T.M., N.M. and H.J.Y. Locomotor studies and two-bottle choice: T.M. and J.J.G. Hargreaves tests: T.M., H.J.Y., J.J.G. and N.M. Ex vivo FSCV: J.H.S. and V.A.A. cFOS counts and immunohistochemistry: T.M., B.R. and J.J.G. Orofacial reactivity and videos: Y.M.V. Surgeries: T.M. Writing (original draft): T.M., M.C.C. and J.A.M. Writing (review and editing): T.M., N.M., C.E.P., J.H.S., B.R., Y.M.V., C.A.M., J.J.G., H.J.Y., V.A.A., M.R.B., M.C.C. and J.A.M. Funding acquisition: V.A.A., M.R.B., M.C.C. and J.A.M. Resources: V.A.A., M.R.B., M.C.C. and J.A.M. Supervision: T.M., M.R.B., M.C.C. and J.A.M.

## Competing interests

The authors declare no competing interests.

## Additional information

**Extended data** is available for this paper at https://doi.org/10.1038/s41593-021-00924-3.

**Supplementary information** The online version contains supplementary material available at https://doi.org/10.1038/s41593-021-00924-3.

**Correspondence and requests for materials** should be addressed to Meaghan C. Creed or Jose A. Morón.

**Peer review information** *Nature Neuroscience* thanks Kate Wassum and the other, anonymous, reviewer(s) for their contribution to the peer review of this work.

**Reprints and permissions information** is available at www.nature.com/reprints.

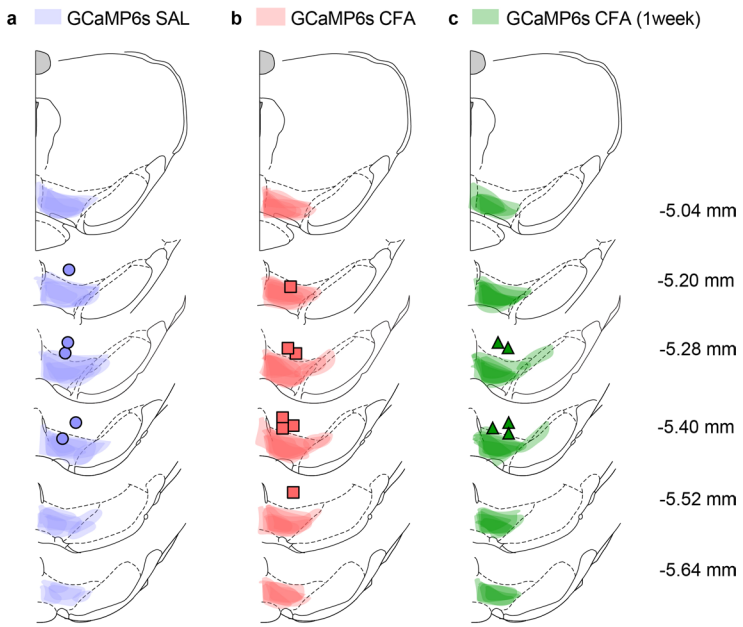


**Extended Data Fig. 1 | Spread of viral expression and fiber optic placement in the VTA. a-c** Spread of overlay of individual animal viral expression and fiber optic placement across the VTA in GCaMP6s injected TH-cre animals.

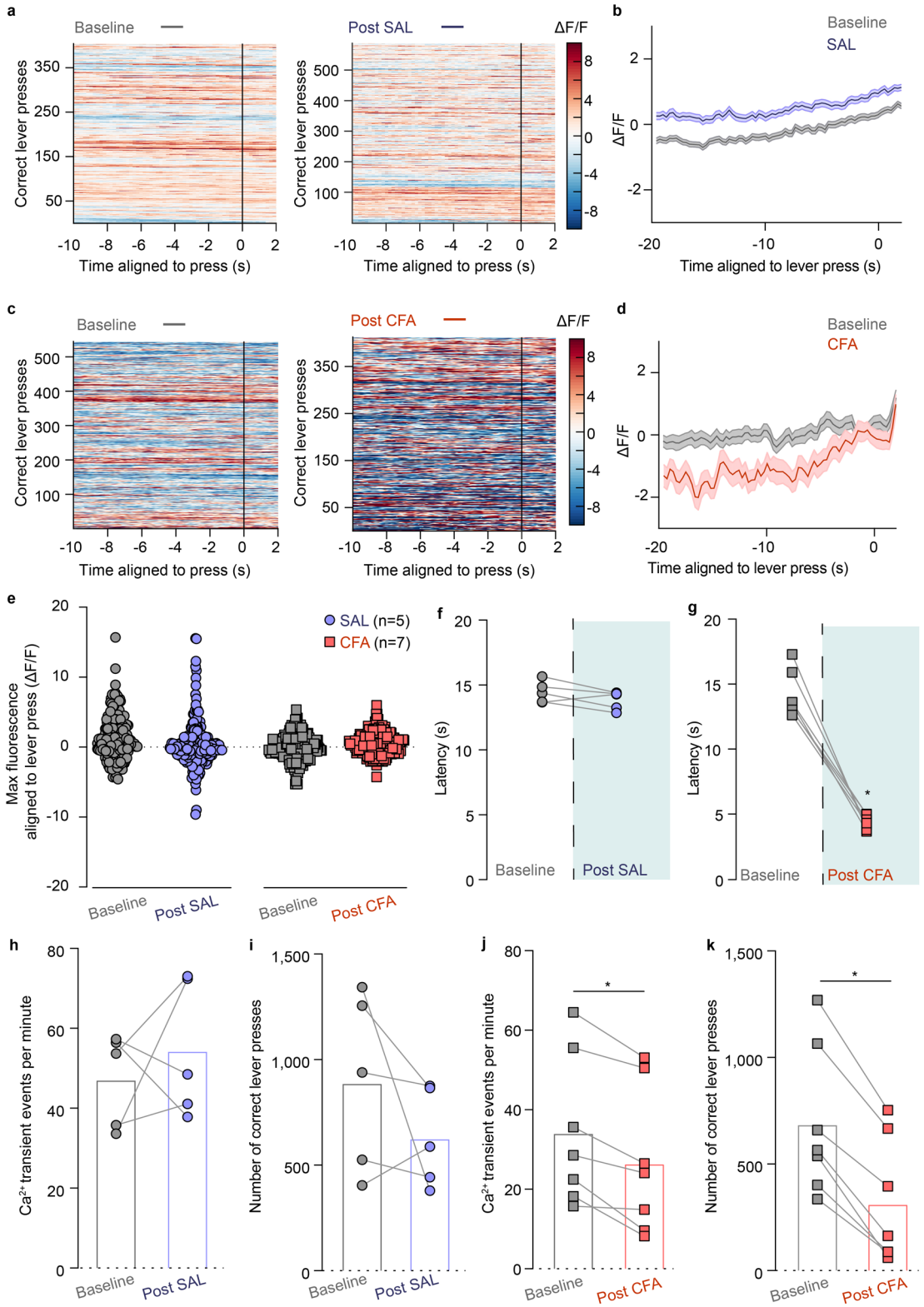


**Extended Data Fig. 2 | See next page for caption.**

**Extended Data Fig. 2 | VTA DA neuron aligned to reward seeking. a**. Representative heat-maps of fluorescence aligned to the lever press (time point 0) for baseline (grey) and post-SAL (blue) PR sessions for same animal. **b**. Mean fluorescence aligned to lever press for baseline (grey) and post-SAL (blue) PR sessions (n = 5 rats; data presented as mean ± s.e.m) **c**. Representative heat-maps of fluorescence aligned to the lever press (time point 0) for baseline (grey) and post-CFA (red) PR sessions for same animal. **d**. Mean fluorescence aligned to lever press for baseline (grey) and post-CFA (red) PR sessions (n = 7 rats; data presented as mean ± s.e.). **e**. Maximum fluorescence aligned to lever press is not altered in either CFA or saline injected animals as compared to their respective baseline. **f**. Saline injection does not alter latency of paw withdrawal to noxious stimulus using Hargraves test. **g**. Latency to withdraw a paw from a noxious stimulus is decreased in CFA, resulting in hyperalgesia (two tailed Wilcoxon test, * p = 0.0156, n = 7 rats). **h**. Transient events per minute of VTA DA neurons throughout the PR sessions are not altered after the injection of saline. **i**. Saline doesn't affect the numbers of correct lever presses during PR session. **j**. CFA decreases overall frequency of VTA DA neurons calcium transients during PR session (two tailed Wilcoxon test, * p = 0.0156, n = 7 rats). **k**. CFA decreases the number of correct lever presses during PR session (two-tailed Wilcoxon test, * p = 0.0156, n = 7 rats).

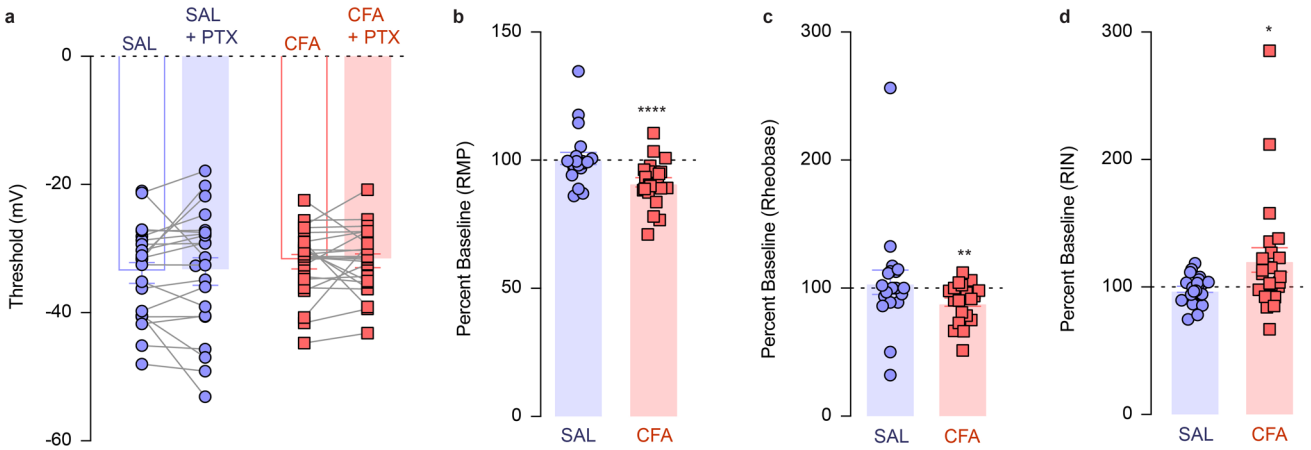


**Extended Data Fig. 3 | Intrinsic excitability of VTA DA neurons is decreased in CFA injected animals. a**. Action potential threshold is not altered in either by CFA or upon application of PTX (n (SAL) = 21 cells from 5 rats, n (CFA) = 23 cells from 4 rats). **b**. Application of picrotoxin (PTX) further depolarized cells from the CFA group while it has no effect on the cells from saline injected animals (one sample t test compared to 100 percent, CFA, **** $p < 0.0001$, n (SAL) = 21 cells from 5 rats, n (CFA) = 23 cells from 4 rats). **c**. Application of picrotoxin (PTX) decreases the amount of current required to depolarize cells to fire an action potential in CFA treated animals (one sample t test compared to 100 percent, CFA, ** $p = 0.0031$, n (SAL) = 20 cells from 5 rats, n (CFA) = 22 cells from 4 rats). **d**. PTX increased input resistance in CFA but not saline treated animals (one sample t test compared to 100 percent, CFA, * $p = 0.0373$, n (SAL) = 21 cells from 5 rats, n (CFA) = 23 cells from 4 rats). The data are presented as the mean ± s.e.m.

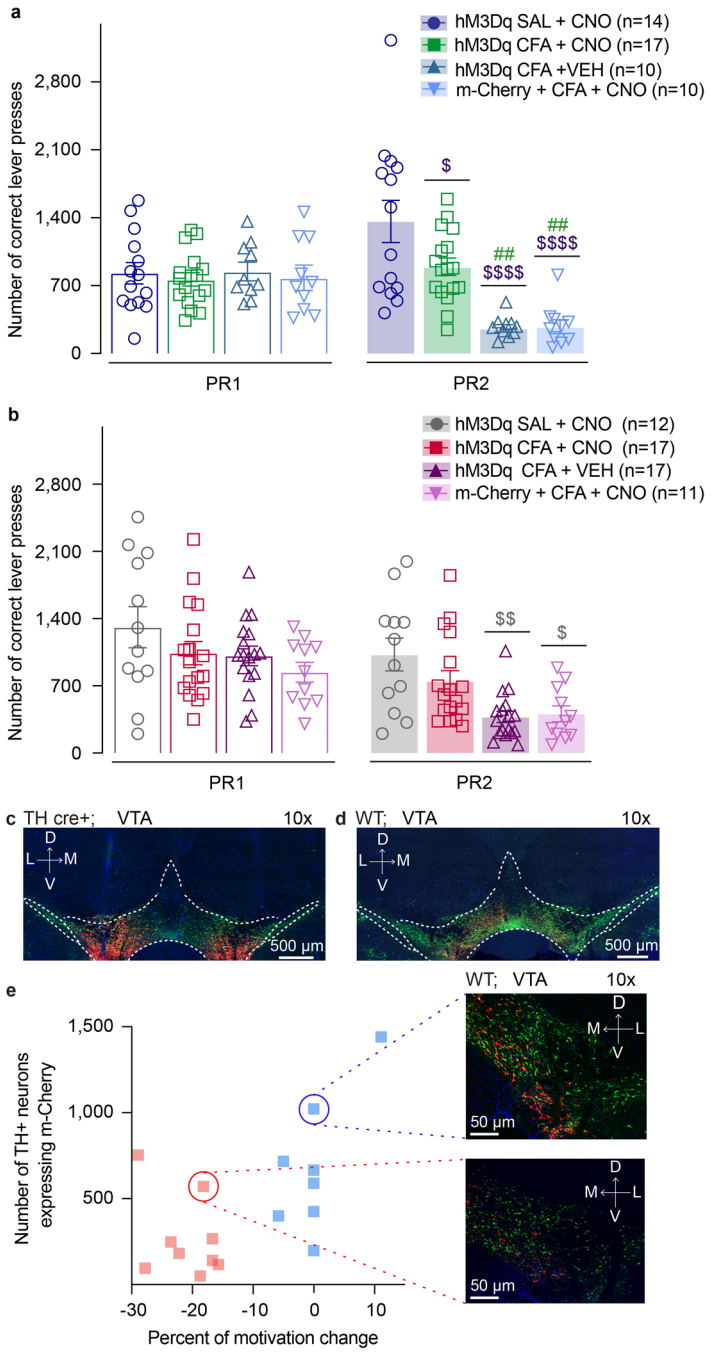


**Extended Data Fig. 4 | See next page for caption.**

**Extended Data Fig. 4 | Chemogenetic activation of VTA DA neurons, or VTA-NAcSh pathway reverses CFA induced decrease in number of correct lever presses for sucrose rewards in PR task. a**. Activation of DA containing neurons in the VTA reverses CFA induced decrease in number of correct lever presses in sucrose PR. Animals injected with control virus and CNO alone showed decrease in the number of correct lever presses after the CFA injection (two-way ANOVA for repeated measures, time: $F_{1, 47} = 3.361$, $p = 0.0731$; interaction (time x treatment): $F_{3, 47} = 21.02$, $p < 0.0001$; Sidak's post hoc between groups during PR2: hM3Dq + CFA + VEH $_{(n=10)}$ versus hM3Dq + SAL + CNO $_{(n=14)}$, $$$$ $p < 0.001$, hM3Dq + CFA + VEH versus hM3Dq + CFA + CNO $_{(n=17)}$, ## $p = 0.002$; m-Cherry + CFA + CNO $_{(n=10)}$ versus hM3Dq + SAL + CNO, $$$$ $p < 0.0001$, m-Cherry + CFA + CNO versus hM3Dq + CFA + CNO, ## $p = 0.0028$), hM3Dq + CFA + CNO versus hM3Dq + SAL + CNO, $ $p = 0.0188$). **b**. Activation of NAcSh projecting VTA neurons reverses CFA induced decrease in number of correct lever presses in sucrose PR. Control CFA animals injected with either CNO or virus alone show decrease in number of correct lever presses in sucrose PR (two-way ANOVA for repeated measures, time: $F_{1, 53} = 87.59$, $p < 0.0001$; interaction (time x treatment): $F_{3, 53} = 4.036$, $p = 0.0117$; Sidak's post hoc during PR2 between the groups: hM3Dq + CFA + VEH $_{(n=17)}$ versus hM3Dq + SAL + CNO $_{(n=12)}$, $$ $p = 0.0021$, m-Cherry + CFA + CNO $_{(n=11)}$ versus hM3Dq + SAL + CNO, $ $p = 0.0116$). The data are presented as the mean ± s.e.m. **c**. Representative coronal section of VTA DREADD expressing neurons. Blue – DAPI; Red – m-Cherry (Gq DREADD); Green – TH (DA neurons). Schematic representation of viral injections for Gq DREADD injected TH cre + rats used for chemogenetic experiments in Fig. 3a–d. **d**. Representative coronal section of VTA Gq DREADD expressing neurons. Blue – DAPI; Red – m-Cherry (Gq DREADD); Green – TH (DA neurons). Schematic representation of viral injections for Gq DREADD injected wild type rats used in chemogenetics experiment in Fig. 3e–k. **e**. Representative images of low viral infection rate (red dotted line) correlated with decrease in motivation (red circle) and high viral infection rate (blue dotted line) correlated with no change in motivation (blue circle) during PR test using intersectional chemogenetics in CFA treated animals.

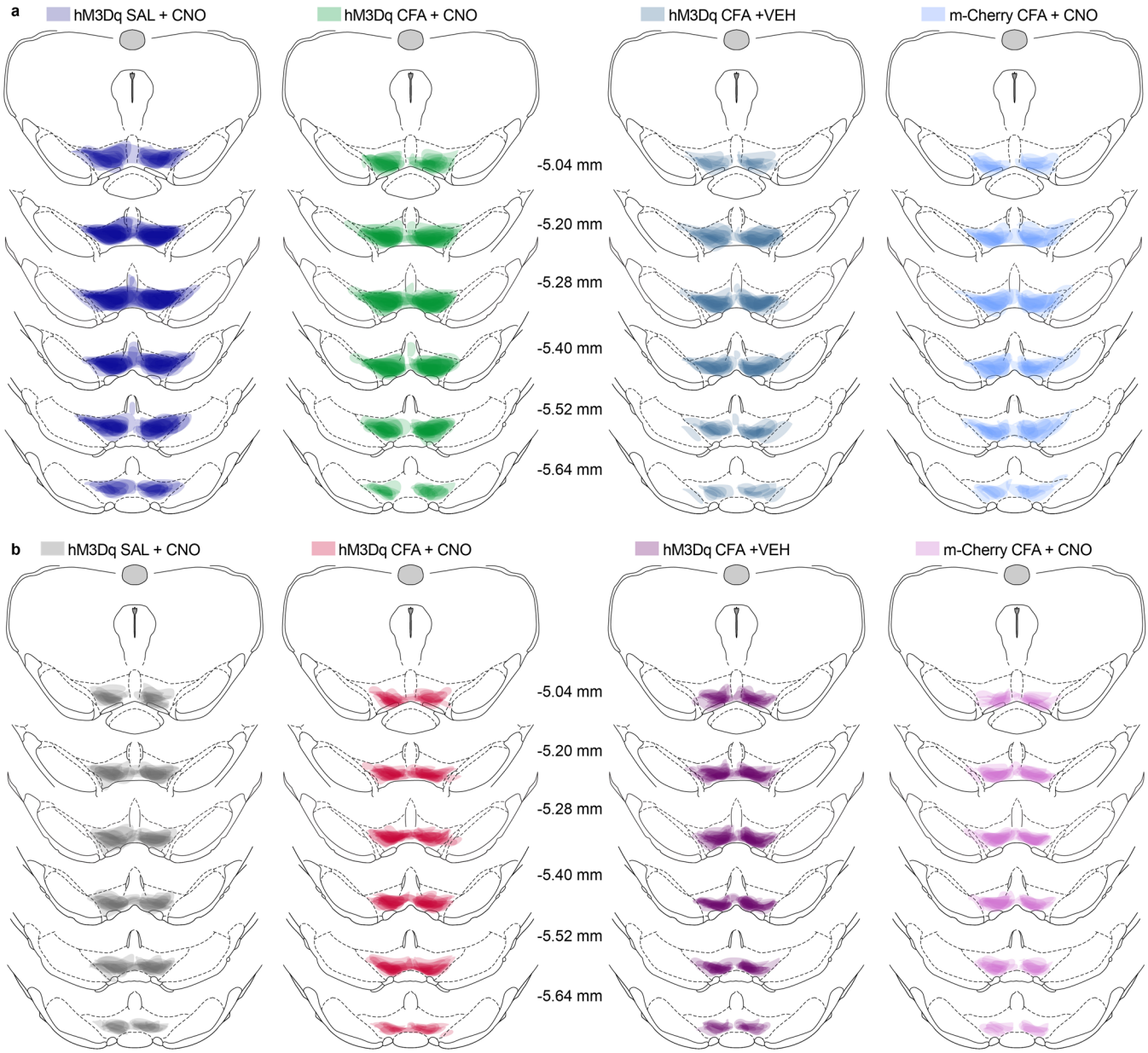


**Extended Data Fig. 5 | Spread of viral expression in the VTA. a**. Spread of overlay of individual animal viral expression across VTA in DREADD and control m-Cherry injected TH-cre animals used in Fig. 3b–d. **b**. Spread of overlay of individual animal viral expression across VTA in DREADD and control m-Cherry injected WT animals used in Fig. 3f–k.

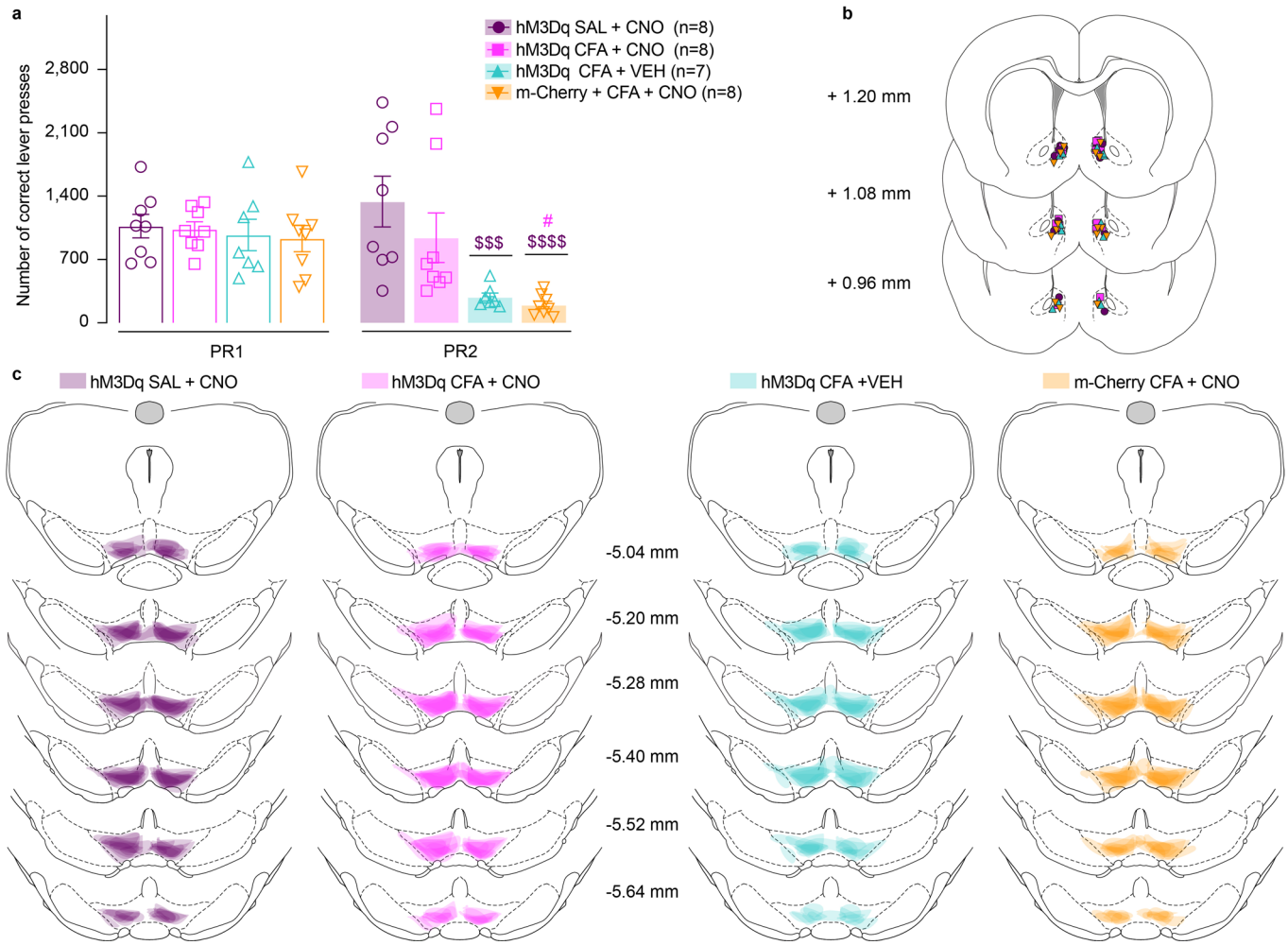


**Extended Data Fig. 6 | Chemogenetic activation of NAcSH projecting VTA DA neurons, prevents CFA induced decrease in number of correct lever presses for sucrose rewards in PR task. a**. Activation of DA containing NAcSh projecting VTA neurons prevents CFA induced decrease in number of correct lever presses in sucrose PR. Animals injected with control virus and CNO alone showed decrease in the number of correct lever presses after the CFA injection (two-way ANOVA for repeated measures, time: $F_{1, 27} = 8.016$, $p = 0.0087$; interaction (time x treatment): $F_{3, 27} = 4.966$, $p = 0.0071$; Sidak's post hoc between groups during PR2: hM3Dq + CFA + VEH $_{(n=7)}$ versus hM3Dq + SAL + CNO $_{(n=8)}$, $$$ $p = 0.0005$; m-Cherry + CFA + CNO $_{(n=8)}$ versus hM3Dq + SAL + CNO, $$$$ $p < 0.0001$, m-Cherry + CFA + CNO versus hM3Dq + CFA + CNO$_{(n=8)}$, # $p = 0.0190$). **b**. Schematic representation of cannula placement in the NAcSh for local delivery of aCSF or CNO. **c**. Spread of overlay of individual animal viral expression across VTA in DREADD and control m-Cherry injected TH-cre animals. The data are presented as the mean ± s.e.m.

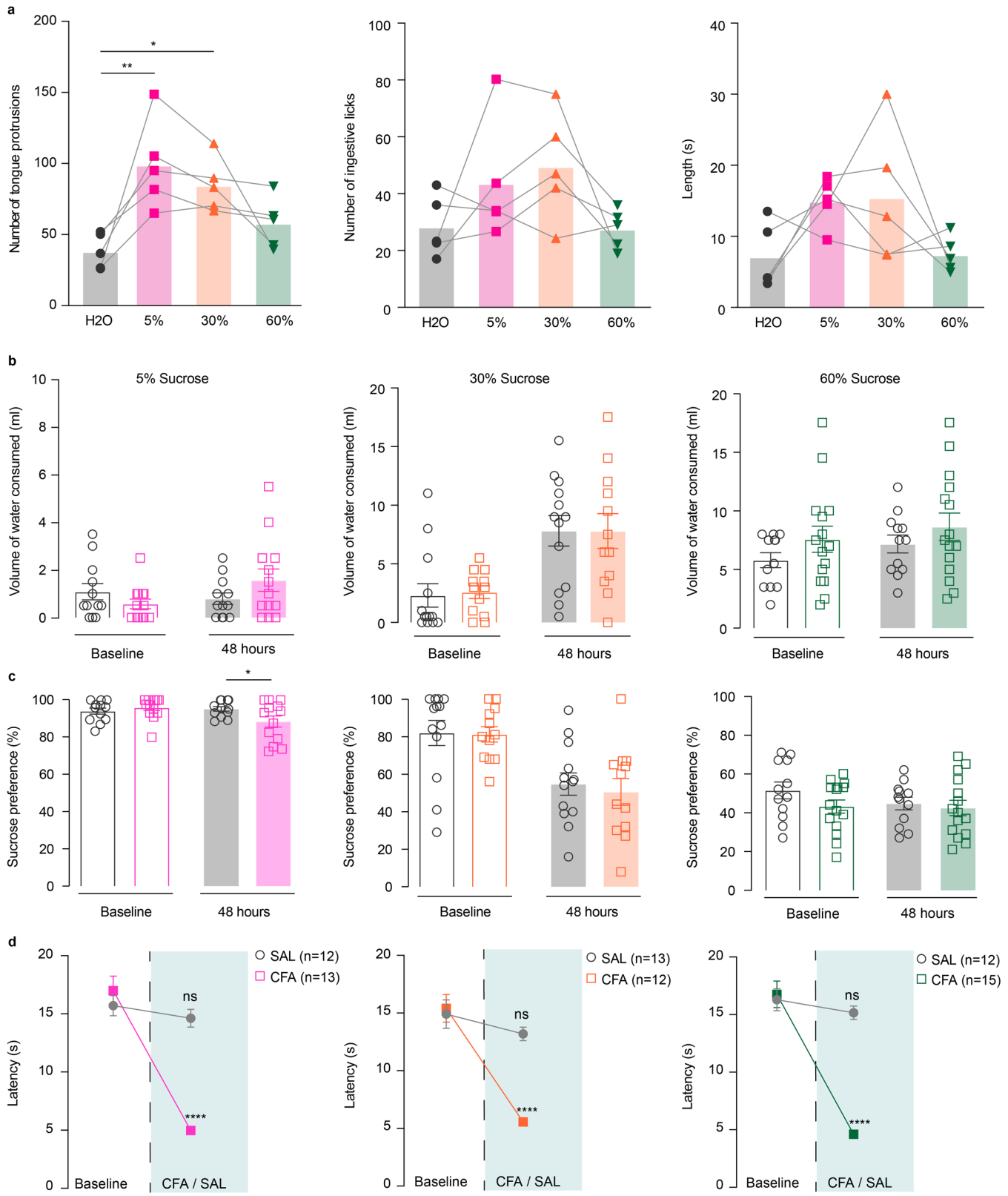


**Extended Data Fig. 7 | See next page for caption.**

**Extended Data Fig. 7 | CFA does not alter intake of water during the sucrose two-bottle choice experiment. a**. 5% and 30% sucrose significantly increased consummatory protrusions as compared to water, with similar trend being seeing with 60% sucrose as well (ANOVA Friedman's test, **** $p < 0.0001$; two-tailed Dunn's multiple comparisons post hoc: 5% sucrose versus water, ** $p = 0.0036$; 30% sucrose versus water, * $p = 0.0423$, $n = 5$ rats). No changes are observed in number of ingestive licks or the length of the lick between different concentrations. **b**. Volume of water consumed is not changed after the CFA injection during either 5% (CFA ($n = 13$ rats), SAL ($n = 12$ rats)), 30% (CFA ($n = 12$ rats) and SAL ($n = 13$ rats)) or 60% (CFA ($n = 15$ rats), SAL ($n = 12$ rats)) sucrose two-bottle choice. **c**. CFA decreases 5% sucrose preference during two-bottle choice (open bars -baseline, filled bars – 48 hours post CFA/SAL. two-way ANOVA for repeated measures, time: $F_{1, 23} = 2.339$, $p = 0.1398$; interaction (time x treatment): $F_{1, 23} = 4.446$, $p = 0.0461$; Sidak's post hoc within group: CFA $_{(n=13)}$ baseline versus 48 hours post CFA, * $p = 0.03$), while it has no effect on 30% or 60% sucrose preference. **d**. CFA decreases latency to withdrawal from a noxious stimulus resulting in hyperalgesia (two-way ANOVA for repeated measures, 5% sucrose (CFA ($n = 13$ rats), SAL ($n = 12$ rats)), time: $F_{1,23} = 91.75$, $p < 0.0001$; interaction (time x treatment): $F_{1,23} = 63.86$, $p < 0.0001$; Sidak's post hoc for each group as compared to the group's baseline session: **** $p < 0.0001$; 30% sucrose (CFA ($n = 12$ rats) and SAL ($n = 13$ rats)) time: $F_{1,23} = 40.71$, $p < 0.0001$; interaction (time x treatment): $F_{1,23} = 20.02$, $p = 0.0002$; Sidak's post hoc for each group as compared to the group's baseline session: **** $p < 0.0001$; 60% sucrose 60% (CFA ($n = 15$ rats), SAL ($n = 12$ rats)) time: $F_{1,25} = 72.34$, $p < 0.0001$; interaction: $F_{1,25} = 43.85$, $p < 0.0001$; Sidak's post hoc for each group as compared to the group's baseline session: **** $p < 0.0001$). The data are presented as the mean ± s.e.m.

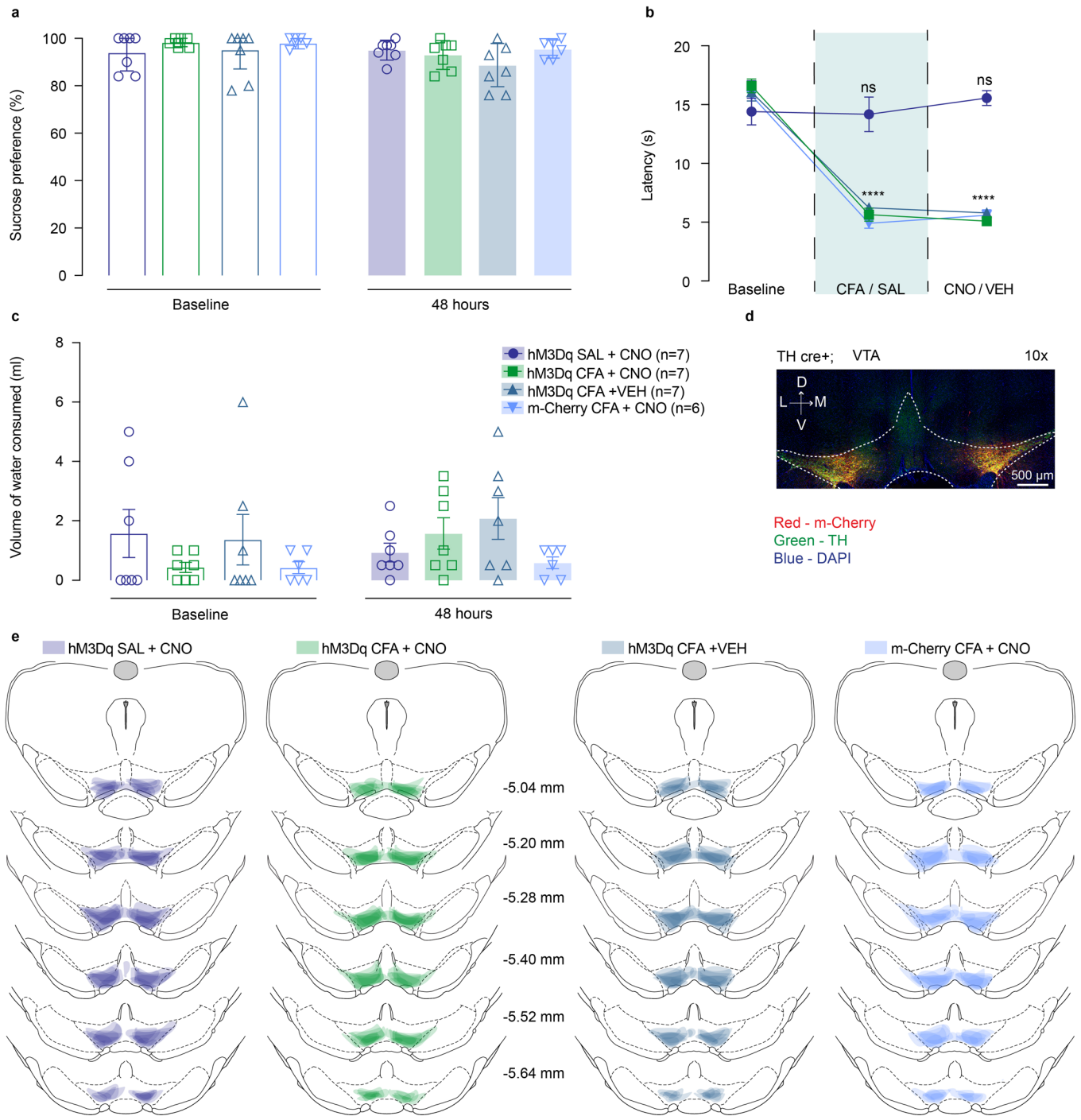


**Extended Data Fig. 8 | Chemogenetic stimulation of VTA DA neurons does not alter water intake in two-bottle choice test. a**. Chemogenetic activation of DA containing neurons in the VTA does not alter sucrose preference in two-bottle choice test. **b**. CFA induced hyperalgesia is not altered by activation of VTA DA neurons (two-way ANOVA for repeated measures, time: $F_{2, 48} = 148.2$, $p < 0.0001$; interaction (time x treatment): $F_{6, 48} = 19.30$, $p < 0.0001$; Sidak's post hoc for each group as compared to the group's baseline session: **** $p < 0.0001$; n (hM3Dq SAL + CNO) = 7 rats, n (hM3Dq CFA + CNO) = 7 rats, n (hM3Dq CFA + VEH) = 7 rats, n (m-Cherry CFA + CNO) = 6 rats). **c**. Chemogenetic activation of DA containing neurons in the VTA does not alter water consumption in two-bottle choice test. **d**. Representative coronal section of VTA DREADD expressing neurons. Blue – DAPI; Red – m-Cherry (Gq DREADD); Green – TH (DA neurons). **e**. Spread of overlay of individual animal viral expression across VTA in DREADD and control m-Cherry injected TH-cre animals. The data are presented as the mean ± s.e.m.

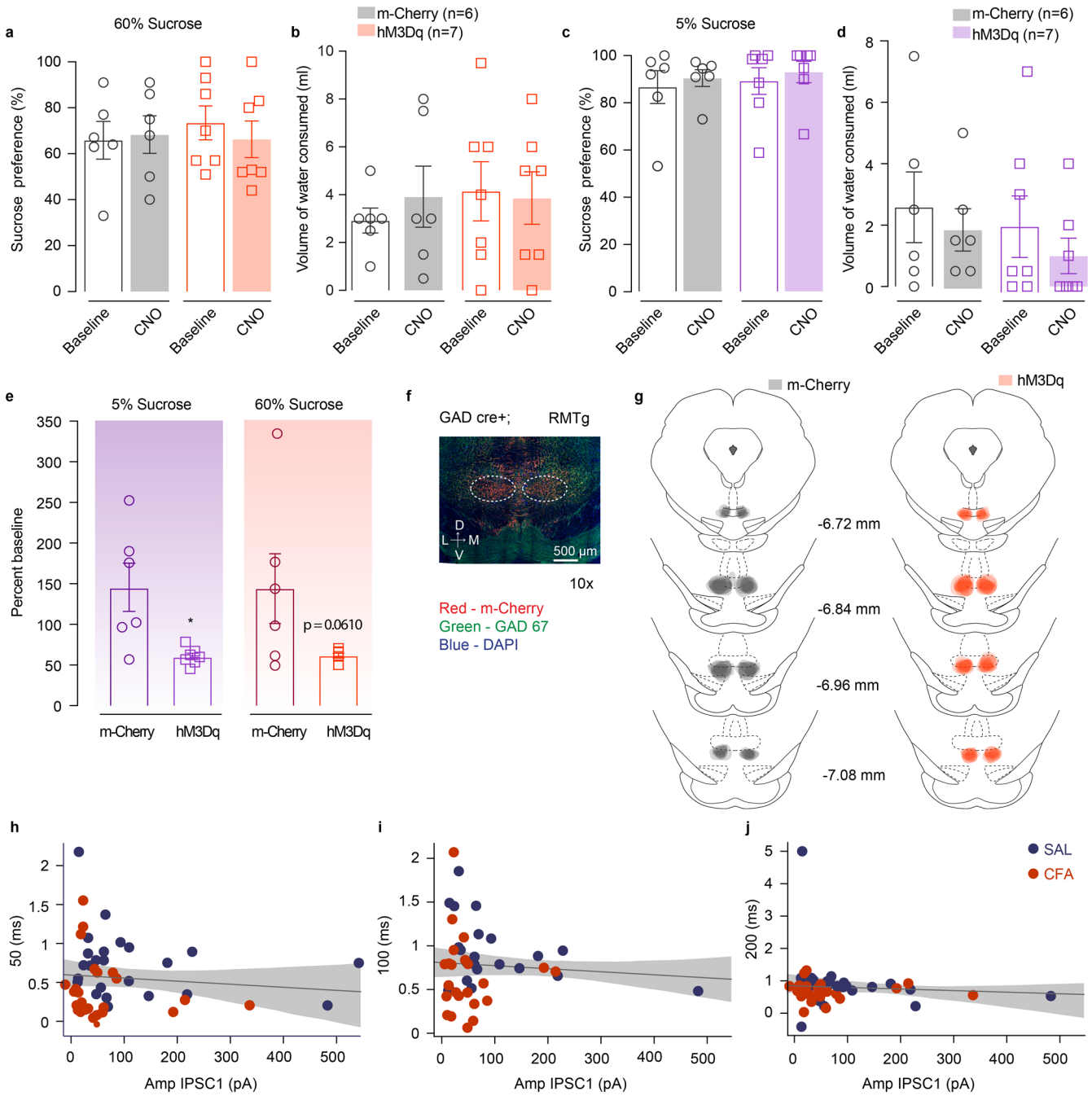


**Extended Data Fig. 9 | Chemogenetic stimulation of RMTg GABA neurons does not alter sucrose preference in two-bottle choice test. a-d**. Chemogenetic activation of RMTg GABA cells does not alter preference for 60% or 5% sucrose or water consumption in two-bottle choice test. **e**. Sucrose consumption presented as percent change of baseline (5% sucrose (n (m-Cherry) = 6 rats, n (hM3Dq) = 7 rats) two tailed unpaired t test, * p = 0.0105; 60% sucrose (n (m-Cherry) = 6 rats, n (hM3Dq) = 7 rats) two tailed unpaired t test p = 0.0610). **f**. Representative coronal section of RMTg Gq DREADD expressing neurons. Blue – DAPI; Red – m-Cherry (Gq DREADD); Green – GAD 67 (GABA neurons). **g**. Spread of overlay of individual animal viral expression across RMTg in DREADD and control m-Cherry injected GAD-cre animals. The data are presented as the mean ± s.e.m. **h-j**. PPR is not correlated with the evoked amplitude of initial response at any inter-pulse interval. The data are presented as regression line and 95% confidence interval.

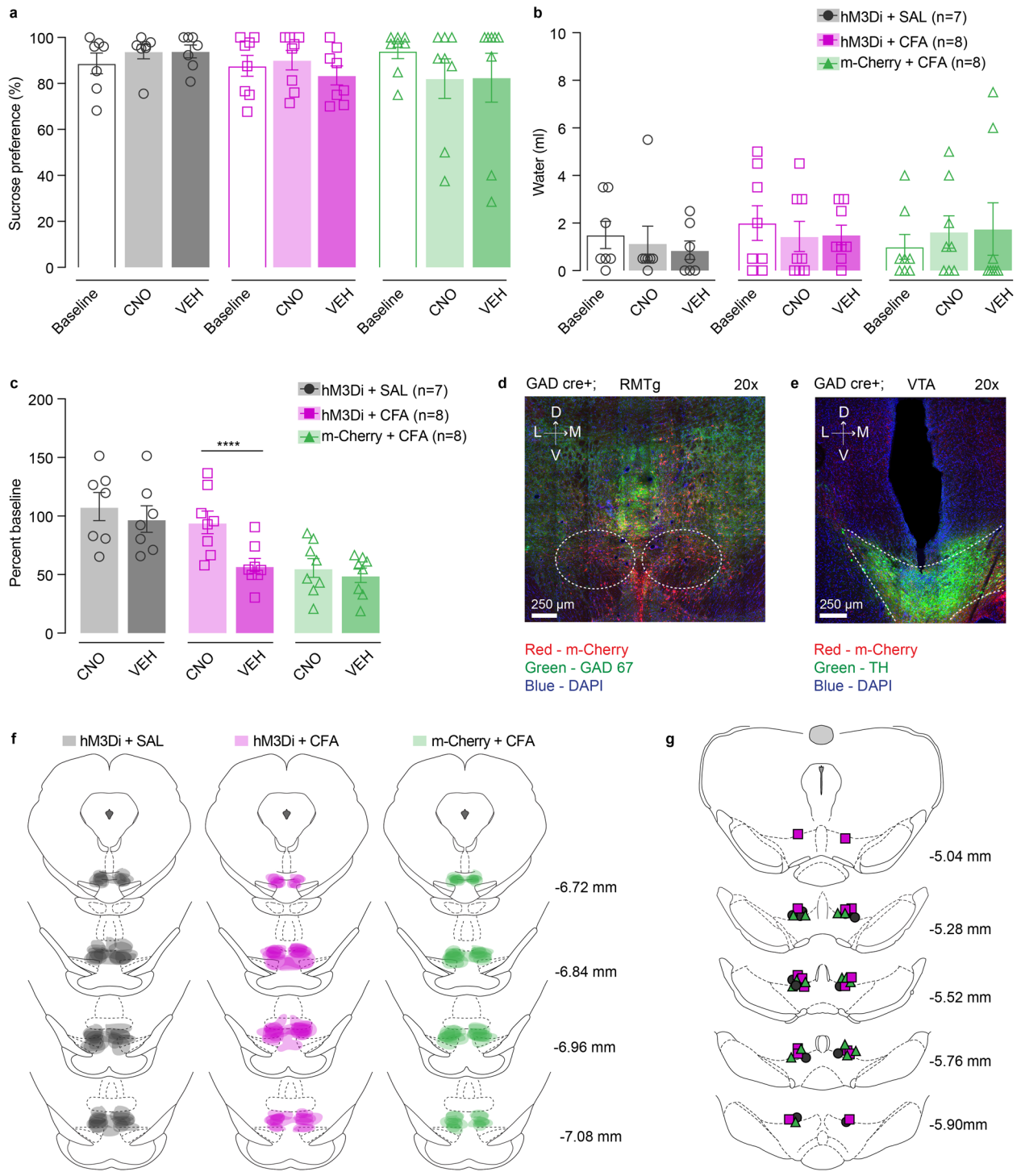


**Extended Data Fig. 10 | Chemogenetic inhibition of RMTg-VTA GABAergic pathway does not alter sucrose preference in two-bottle choice test.** **a-b**. Chemogenetic inhibition of RMTg GABA cells projecting to VTA does not alter sucrose preference or water consumption in two-bottle choice test. **c**. Sucrose consumption presented as percent change of baseline (two-way ANOVA for repeated measures, time: $F_{1,20}=20.89$, $p=0.0002$; interaction (time x treatment): $F_{2,20}=6.236$, $p=0.0079$; Sidak's post hoc within group: hM3Di + CFA + $CNO_{(n=8)}$ versus hM3Di + CFA + $VEH_{(n=8)}$, **** $p<0.0001$) **d**. Representative coronal section of RMTg Gi DREADD expressing neurons. Blue – DAPI; Red – m-Cherry (Gi DREADD); Green – GAD 67 (GABA neurons). **e**. Representative coronal section of cannula placement in the VTA. Blue – DAPI; Red – m-Cherry (Gi DREADD); Green – TH (DA neurons). **f**. Spread of overlay of individual animal viral expression across RMTg in DREADD and control m-Cherry injected GAD-cre animals. **i**. Schematic representation of cannula placement in the VTA for local delivery of aCSF or CNO. The data are presented as the mean ± s.e.m.

nature portfolio

Corresponding author(s): Jose A. Morón; Meaghan C. Creed

Last updated by author(s): Aug 12, 2021

# Reporting Summary

Nature Portfolio wishes to improve the reproducibility of the work that we publish. This form provides structure for consistency and transparency in reporting. For further information on Nature Portfolio policies, see our Editorial Policies and the Editorial Policy Checklist.

## Statistics

For all statistical analyses, confirm that the following items are present in the figure legend, table legend, main text, or Methods section.

| n/a | Confirmed |
|---|---|
| ☐ | ☒ The exact sample size (*n*) for each experimental group/condition, given as a discrete number and unit of measurement |
| ☐ | ☒ A statement on whether measurements were taken from distinct samples or whether the same sample was measured repeatedly |
| ☐ | ☒ The statistical test(s) used AND whether they are one- or two-sided<br>*Only common tests should be described solely by name; describe more complex techniques in the Methods section.* |
| ☒ | ☐ A description of all covariates tested |
| ☐ | ☒ A description of any assumptions or corrections, such as tests of normality and adjustment for multiple comparisons |
| ☐ | ☒ A full description of the statistical parameters including central tendency (e.g. means) or other basic estimates (e.g. regression coefficient) AND variation (e.g. standard deviation) or associated estimates of uncertainty (e.g. confidence intervals) |
| ☐ | ☒ For null hypothesis testing, the test statistic (e.g. *F*, *t*, *r*) with confidence intervals, effect sizes, degrees of freedom and *P* value noted<br>*Give P values as exact values whenever suitable.* |
| ☒ | ☐ For Bayesian analysis, information on the choice of priors and Markov chain Monte Carlo settings |
| ☒ | ☐ For hierarchical and complex designs, identification of the appropriate level for tests and full reporting of outcomes |
| ☒ | ☐ Estimates of effect sizes (e.g. Cohen's *d*, Pearson's *r*), indicating how they were calculated |

*Our web collection on statistics for biologists contains articles on many of the points above.*

## Software and code

Policy information about availability of computer code

| | |
|---|---|
| Data collection | Fiber photometry data was collected using TDT, RZ5P system and the envelopes of the 531-Hz and 211-Hz signals were extracted in real-time by the TDT program Synapse Version 95 at a sampling rate of 1017.25 Hz.<br>Patch-clamp electrophysiology data acquisition was completed using Clampex 11.4 software (Molecular Devices).<br>For ex vivo fast-scan cyclic voltammetry data was collected with a modified electrochemical headstage (CB-7B/EC retrofit with 5 MΩ resistor) using a Multiclamp 700B amplifier (Molecular Devices) after being low-pass filtered at 10 kHz and digitized at 100 kHz using custom-written software Igor Pro 7 (version 7.0.6.1, Wavemetrics) running mafPC 2019 software (courtesy of M.A. Xu-Friedman)<br>For operant conditioning experiments data were collected using Med Associates operant-conditioning chambers (Med Associates, Fairfax, VT Med-PC 5 software).<br>For thermal hyperalgesia we used Hargreaves Plantar Test (IITC Life Science) to collect the data.<br>For locomotor studies AnyMaze 6.06 (64-bit) behavioral tracking software was used |
| Data analysis | For statistical analysis GraphPad Prism 8.1.0 (Graph Pad Software, Inc., USA), MatLab, Image J 1.53a and custom-written analysis software in Igor Pro 7 were used. Custom MatLab code for photometry analysis and custom-written Igor Pro 7 and mafPC for ex vivo fast-scan cyclic voltammetry are made available via Github and Bitbucket. Access links are included in Code and software availability section of the manuscript |

For manuscripts utilizing custom algorithms or software that are central to the research but not yet described in published literature, software must be made available to editors and reviewers. We strongly encourage code deposition in a community repository (e.g. GitHub). See the Nature Portfolio guidelines for submitting code & software for further information.

## Data

Policy information about availability of data

All manuscripts must include a data availability statement. This statement should provide the following information, where applicable:

- Accession codes, unique identifiers, or web links for publicly available datasets
- A description of any restrictions on data availability
- For clinical datasets or third party data, please ensure that the statement adheres to our policy

The data collected during this study are available from the corresponding author upon request.

# Field-specific reporting

Please select the one below that is the best fit for your research. If you are not sure, read the appropriate sections before making your selection.

☒ Life sciences ☐ Behavioural & social sciences ☐ Ecological, evolutionary & environmental sciences

For a reference copy of the document with all sections, see nature.com/documents/nr-reporting-summary-flat.pdf

# Life sciences study design

All studies must disclose on these points even when the disclosure is negative.

| | |
|---|---|
| Sample size | No statistical methods were used to per-determine sample sizes but our sample sizes are similar to those reported in previous publications (PMID: 30878290; PMID: 26338332; PMID: 27170097) |
| Data exclusions | No data was excluded from analysis |
| Replication | All experiments were performed at least twice, including each treatment condition to prevent an unspecific day/condition effect. Each replicate experiment successfully recapitulated original findings |
| Randomization | Treatment groups were randomly assigned to animals prior to testing. |
| Blinding | All investigators were blinded to group allocation during data collection and analysis. |

# Reporting for specific materials, systems and methods

We require information from authors about some types of materials, experimental systems and methods used in many studies. Here, indicate whether each material, system or method listed is relevant to your study. If you are not sure if a list item applies to your research, read the appropriate section before selecting a response.

## Materials & experimental systems

| n/a | Involved in the study |
|---|---|
| ☐ | ☒ Antibodies |
| ☒ | ☐ Eukaryotic cell lines |
| ☒ | ☐ Palaeontology and archaeology |
| ☐ | ☒ Animals and other organisms |
| ☒ | ☐ Human research participants |
| ☒ | ☐ Clinical data |
| ☒ | ☐ Dual use research of concern |

## Methods

| n/a | Involved in the study |
|---|---|
| ☒ | ☐ ChIP-seq |
| ☒ | ☐ Flow cytometry |
| ☒ | ☐ MRI-based neuroimaging |

## Antibodies

Antibodies used

Mouse anti-TH, Millipore, MAB318; RRID:AB_2201528; dilution 1:1000
Rabbit anti- mCherry; ab167453, Abcam, Cambridge, MA; RRID: AB_2571870; dilution 1:500
Mouse anti-GAD67, 1:5,000; MAB5406, EMDMillipore, Billerica, MA; RRID:AB_2278725; dilution 1:5000
Biotin-SP Donkey anti-Mouse; Cat. 715-065-150; RRID: AB_2307438; Jackson; dilution 1:200
Donkey anti-Mouse AF488; Cat. 115-545-150; RRID: AB_2340846; Jackson; dilution 1:200
Donkey anti-Rabbit Cy3; Cat. 711-165-152; RRID: AB_2307443; Jackson; dilution 1:200
Streptavidin AF488; Cat. 016-540-184; RRID: AB_2337249; Jackson; dilution 1:200
Rabbit anti-cFos, ab190289, Abcam; dilution 1:2000
Chicken anti-mCherry, ab205402, Abcam; dilution 1:500
Donkey anti-Rabbit; RRID: AB_2340616; Jackson; dilution 1:200

Donkey anti-Chicken; RRID: AB_2340363; Jackson; dilution: 1:200

Validation

Mouse anti-TH (e.g. PMID 19748892)
Rabbit anti- mCherry (e.g. PMID: 30984001)

## Animals and other organisms

Policy information about studies involving animals; ARRIVE guidelines recommended for reporting animal research

| | |
|---|---|
| Laboratory animals | Male and female Long Evans Wild Type, TH-cre and GAD-cre rats (250-350g for behavioral studies), and DAT IRES-cre mice crossed with Cre driven expression of ChR2 mice (AiCop4) were used for this study. All animals were 4 to 10 weeks old at the beginning of the experiments. Rats were group housed with two to three animals per cage on a 12/12 hours dark/light cycle (lights on at 7:00 AM) and acclimated to the animal facility holding rooms for at least 7 days before any manipulation. All experiments were performed during the light cycle. Mice were housed up to 4 animals per cage. The temperature for the holding rooms of all animals ranged from 69-75°F while the humidity was between 30-70%. |
| Wild animals | The study did not involve wild animals. |
| Field-collected samples | This study did not involve samples collected from the field. |
| Ethics oversight | All procedures were approved by Washington University and the National Institute on Alcohol Abuse and Alcoholism (NIAAA) Animal Care and Use Committee in accordance with the National Institutes of Health Guidelines for the Care and Use of Laboratory Animals. |

Note that full information on the approval of the study protocol must also be provided in the manuscript.